B-cation ordering and dielectric properties of relaxor ferroelectric $Pb(Sc_{1/2}Nb_{1/2})O_3$

Jonas Said Baazi

Preface

This Master thesis is a continuation of the Master project *"B- cation ordering in relaxor ferroelectric perovskites"* dated December 2012 [7]. It represents the final task where students are given the freedom to conduct their own research. From the beginning of the project work I was presented to a lot of new theory which have been interesting and motivating. The theory in this thesis has been rewritten to include important facts for this thesis and contains also much of the same theory from the project work. The end of the theory section concerning cation ordering and its effect on the lattice constant, and the theory concerning the ordering effect on dielectric properties, is partially a result after intensive literature study. The experimental results in in this thesis, demanded further literature study and the use of visualization tools, to be explained. I therefore hope the reader will find these sections especially useful when interpreting the results. Furthermore, the reader is advised to look back on the theory to have a full understanding of both the results and the reasons for the methods used in this thesis. The literature list also contain a large variety of both experimental work and theoretical studies which should be investigated by the curious reader.

In addition to studying both old and new literature, this thesis has involved a great amount of laboratory work. Students following the nanotechnology master program, including myself, are not presented to significant laboratory work during their five years of studying. Therefore, to be given the freedom to conduct own experiments has been both challenging and motivating.

I would like to thank Professor Tor Grande and the "Ferro- group" at NTNU for great feedback during my last two semesters at NTNU (2012-2013). I have received great knowledge about what it takes to be a good researcher, and been introduced to science and equipment that have challenged me in a motivating way. Likewise, the weekly meetings with our group, which served as an arena to bring up and discuss important scientific questions, have been helpful on my way to completing this final task.

I would also like to thank Senior Engineer Julian Tolchard for assisting me the X-Ray Diffraction analysis and SEM imaging, postdoctoral fellow Maxim Morosov for helping me with the dielectric spectrometer, and associate professor Sverre M. Selbach for taking time to answer my questions when I show up at his office unannounced. And last, but not least, a big thanks to my fellow students following the nanotechnology master program, "kull- 08", for great support and motivation throughout these five years of studying.

Abstract

Molten salt synthesis and solid state synthesis were used to make relaxor ferroelectric $Pb(Sc_{1/2}Nb_{1/2})O_3$,abbreviated PSN in most literature. Many studies have previously been conducted on this material to obtain so called B- cation ordering of the scandium and niobium atoms. The reason for the interest in this is the ordering effect on the dielectric properties. To obtain cation ordering, this material is typically annealed for longer times in a temperature interval which is quite high (approx. 940°C-1200°C). In this thesis we studied the molten salt synthesis of PSN using a 0.5NaCl-0.5KCl salt combination and its effect on ordering when varying different parameters. The goal was to synthesize cation ordered PSN at lower temperatures than before. However, we were able to synthesize phase pure PSN, but no cation ordering could be observed. The syntheses were carried out using two different routes, both with and without a $ScNbO_4$ precursor, the first referred to as the *Wolframite method*. Although no B- cation ordering could be observed, there were other interesting observations. When using the precursor, the purities were consequently higher. At least one unknown secondary phase was present in almost all syntheses without the precursor. In addition, different temperatures, times, and heating- and cooling rates had a similar influence on the particle sizes. The particle sizes increased with increasing time and synthesis temperature, both with and without the precursor. Fast and slow heating rates resulted in smaller and bigger PSN particles respectively. The same tendency was observed for the measured crystallite sizes. From the results of both crystallite and particle sizes, the importance of particle sizes on reaction rates were revealed as the *Wolframite method* showed a slower reaction rate. This is thought to be related to the large $ScNbO_4$ precursor particles acting as PSN nucleation sites. The calculated lattice constants were in the lower range of PSN literature values but not as low as for cation ordered PSN. It was also found that the PSN powder with the smallest calculated crystallite sizes also showed the smallest lattice constants, but no significant correlation was found between them. The ordering effect on the crystal lattice is visualized and used to explain both the smaller lattice constant of ordered PSN, and the ordering effect on the dielectric properties.

To perform dielectric measurements, solid state synthesis was first used to make dense PSN pellets. Several test samples were made until the final PSN pellets reached 92.5% to 94.5% of theoretical density. The purity of the PSN pellets was established from XRD which were all phase pure after using a 4wt% PbO excess. The excess PbO showed its importance in both maintaining the PSN stoichiometry and as a sintering aid. All samples were additionally annealed at different temperatures and times in an attempt to increase the degree of ordering. However, XRD data showed no signs of cation ordering after annealing but, dielectric spectroscopy showed a clear lowering of the dielectric permittivity maxima (ε_m) and the permittivity maxima temperature (T_m). According to literature, this can be caused by both ordering and Pb vacancies in the crystal lattice. The frequency dependence was however

larger after annealing, which is not expected for ordered PSN. The lowering of T_m and ε_m, and the increasing frequency dependence is therefore believed to be caused by PbO evaporation. Both experimental results and theory supporting this will be presented, and its effect on the dielectric properties is discussed.

Sammendrag

Saltsmeltesyntese og fastoffsyntese ble brukt til å lage relaxor ferroelektrisk $Pb(Sc_{1/2}Nb_{1/2})O_3$, ofte forkortet til PSN. Tidligere studier på dette materialet har vært utført for å oppnå såkalt kation ordning på B- plass av scandium og niob. Interessen for dette er effekten ordningen har vist seg å ha på de dielektriske egenskapene til materialet. For å oppnå kation ordning er det kjent at materialet må varmebehandles over lengre tid ved høye temperaturer (ca. 940°C-1200°C). I dette studiet har vi studert saltsmeltesyntese av PSN ved bruk av en 0.5NaCl-0.5KCl saltkombinasjon og dens påvirkning på kation ordning ved å variere forskjellige parametere. Målet var å kunne syntetisere kation ordnet PSN ved lavere temperaturer enn tidligere. Dette viste seg imidlertid vanskelig da vi kun var i stand til å lage uordnet PSN. Syntesene ble gjennomført ved å følge to ulike ruter, med og uten en $ScNbO_4$ forløper, hvor den første ruten er referert til som «*Wolframite method*». Selv om kation ordning ikke kunne oppnås var det andre interessante observasjoner. Når forløperen ble brukt, resulterte det konsekvent i større PSN partikler. I tillegg ble det observert urenheter i nesten alle synteser når forløperen ikke ble brukt. Forskjellige syntesetider, temperaturer og oppvarmings- og nedkjølingshastigheter viste en lik effekt på partikkelstørrelsen. Partikkelstørrelsen økte med temperatur og syntesetid. I tillegg viste det seg at rask og sakte oppvarmingshastighet resulterte i henholdsvis små og store PSN partikler. Den samme tendensen ble funnet igjen i de målte krystallittstørrelsene. Både partikkelstørrelsene og krystallittstørrelsene synligjorde effekten av partikkelstørrelse på reaksjonshastigheten. «*Wolframite method*» viste saktere reaksjonshastighet sammenliknet med den andre ruten og dette ble antatt å skyldes de større forløperpartiklene og deres funksjon som nukleeringssentere. De kalkulerte gitterkonstantene var i det nedre sjikt av rapporterte litteraturverdier for PSN, men ikke så lave som for ordnet PSN. De laveste gitterkonstantene ble funnet for de laveste krystallittstørrelsene men ingen signifikant korrelasjon kunne trekkes ut ifra det. Ordningens påvirkning på krystallstrukturen er illustrert i denne oppgaven for å komme med forslag til hvorfor ordnet PSN har en mindre gitterkonstant.

For å kunne gjøre dielektriske målinger, ble fastoffsyntese og sintring brukt til å lage faste PSN pellets. Det ble utført flere testforsøk inntil pelletene oppnådde en tetthet på 92.5% til 94.5% av teoretisk tetthet. Renheten kunne måles ved bruk av XRD og alle var faserene etter å ha tilsatt et 4vkt% blyoverskudd under sintring. Blyoverkudd viste seg viktig både for å kunne opprettholde støkiometrien og som en sintringshjelp. Etter sintring ble prøvene varmebehandlet i et forsøk på å oppnå kation ordning. Røntgendiffraksjon viste imidlertid ingen tegn til superrefleksjoner, men dielektrisk spektroskopi viste en klar nedgang i både den dielektriske konstanten (ε_m) og temperaturen for det dielektriske maksimum (T_m). I følge litteratur kan dette skyldes både kation ordning i tillegg til blyvakanser i krystallstrukturen. Frekvensavhengigheten var imidlertid høyere etter varmebehandling, noe som ikke er et tegn på ordning. Det er derfor foreslått at de observerte endringer i dielektriske egenskaper

skyldes PbO fordampning. Både eksperimentelle resultater og teori som støtter oppunder dette er presentert, og hvordan dette kan påvirke de dielektriske egenskapene er diskutert.

Contents

1. Introduction

1.1 Motivation

Dielectric materials are divided into piezoelectric, pyroelectric and ferroelectric materials [1, 9, 10]. This is illustrated in Figure 1.1.1 which shows the relationship between the three different materials. Ferroelectric materials are a subclass of pyroelectric materials which are a subset of piezoelectric materials. These materials are characterized by a non-centrosymmetric point group [1]. An example of such a group is a tetrahedral group. The lack of a center of symmetry is what makes it non- centrosymmetric [1]. ZnO and ZnS are examples of materials that are piezoelectric due to a tetrahedral group. The origin and criterion for a material to be piezoelectric is the non- centrosymmetric point group, although many non- piezoelectric materials do have a non- centrosymmetric point group [1].

When a mechanical force is applied to a piezoelectric material, the non- centrosymmetry results in a charge separation, a voltage proportional to the force. In some piezoelectric materials, the direction of the applied force may be of importance [1, 9]. By applying a force along a tetrahedral bond a charge separation is induced, but when the force is applied perpendicular to a tetrahedral edge no voltage can be measured.

Touch screen devices, active vibration control in skis and actuators like AFM that requires high accuracy all takes advantage of piezoelectricity [10]. Pyroelectric materials are affected by mechanical deformation like piezoelectric materials in addition to being sensitive to temperature changes. This is a result of a temperature dependent spontaneous polarization, and the reason why pyroelectric materials are widely used in infrared radiation detectors and sensors [1]. In Ferroelectric materials the polarization direction can be switched by applying an external electric field [1]. This behavior is typically illustrated by a hysteretic response. Also, near the Curie- temperature T_C, the phase transition temperature, ferroelectric materials display a large dielectric constant. For the two reasons mentioned above, these materials are preferred for use in capacitors and memory devices.
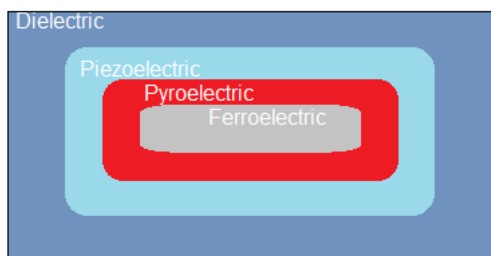
Figure 1.1.1 Illustration of relationship between piezoelectrics, pyroelectrics and ferroelectrics.

Ferroelectric materials can be divided into different groups of materials, one of them complex perovskites which have been studied for a long time, the relaxor family [3, 11]. These materials have many similar properties to classic ferroelectric materials in addition to properties that are still being investigated [11]. A typical ferroelectric relaxor is the $Pb(Mg_{1/3}Nb_{2/3})O_3$ perovskite. Actuators made from PMN were used in the Hubble Telescope 2 to be able to control tilt mirrors for optimal use [11]. The reason for this is the excellent electrostrictive properties of PMN over a large temperature range [12]. All dielectric and non-conductive materials are affected by an external electric field to some extent, and this is called electrostriction. When an external electric field is applied, the dimensions of the material changes [12, 13]. This property is not to be confused with piezoelectricity as the direction and polarity of the applied field has no effect on the mechanical distortions, nor can an electrostrictive material induce a voltage when subjected to a mechanical force. When an external field is applied, electrostriction causes an expansion of the material in the direction of the applied field while it contracts in the orthogonal directions. This property is explained by alignment of charges in the field direction and applies to both centrosymmetric and non-centrosymmetric crystals. Electrostriction can be viewed as a small inverse piezoelectric effect. However, piezoelectric materials deform linearly with the applied field and thereby differs from electrostrictive materials [12, 13].

When comparing ferroelectric relaxors with classic ferroelectric materials, there is a great difference in the temperature dependence of the dielectric constant. Classic ferroelectric materials display a sharp and narrow peak at the phase transition temperature, while relaxors show a larger and broader dielectric dispersion [1]. This is why they are sometimes called ferroelectrics with a diffuse phase transition [3]. Even more interesting is the fact that the temperature at which the dielectric constant is at its maximum, T_m, is frequency dependent [3].

Even though relaxors are called ferroelectrics with a diffuse phase transition, an actual phase transition does not occur. The crystal structure of the relaxors remain cubic both above and below T_m. However, relaxors are associated with ordered nano regions which are polar and dynamic ergodic below the Burns temperature T_B [3]. At this point, they are polar nano regions (PNR) with random dipole moment directions until they become frozen at lower temperatures ,and the relaxor enters a non- ergodic or a ferroelectric state [3]. The physical consequence of the reduced mobility of PNR upon cooling is a shift in T_m depending on the frequency of the applied electrical field. At high frequencies the dielectric maximum occurs at higher temperatures at which the PNR, which exist to some extent in all relaxors, are dynamic [3].

Studies on $Pb(Sc_{1/2}Ta_{1/2})O_3$ (PST) by Setter and Cross showed that thermal annealing is a way to modify the B- cation ordering, in this case the ordering between scandium and tantalum ions [4, 14]. This meaning that the size of the nano domains could be increased by thermal treatment. The study showed that the degree of ordering also had a large effect on both the

dielectric and piezoelectric properties. What they observed was that the ordering caused the relaxor to have similar properties to a classic ferroelectric material at the phase transition temperature, with a sharp peak at T_m indicating the transition from ferroelectric to paraelectric [14]. This has also been confirmed by later studies on the same material [15]. However, ordering does not have the same effect on all relaxors. While some show an increasing dielectric constant, others show a lowering, but common for them all is the ordering effect on the frequency response. For increasing degrees of order, the frequency dependence of T_m is reduced [5, 14, 16].

From the above considerations a conclusion can be made that these materials need further investigation. Both the mechanism of ordering and its effect on the dielectric properties of these materials are not completely understood, although there are several ideas presented in the literature describing ordering in relaxors. Two models describing ordering, the space charge model and the charge balanced random site model [3, 16, 17], will be looked into in this thesis.

Dielectric properties are greatly influenced by the atomic arrangement of B- cations, but also, the B- cations affect the synthesis conditions needed to obtain ordering [18]. To be able to predict the resulting ordering and the synthesis conditions needed, the sizes and charges of the B- cations has been shown highly relevant. Studies show the existence of a so called order- disorder temperature that separates an ordered and disordered atomic arrangement [18, 19]. For PMN, this is located below the temperature where cation diffusion is possible, which means that a different approach to synthesis must be considered [20]. In PSN on the other hand, the size and charge differences between the B- cations are believed to increase the order- disorder temperature to a higher level so that ordering can be obtained by annealing in a temperature interval where the order- disorder temperature represents the higher limit [3, 5, 18].

In 1982 Swartz *et al.* introduced a new method for synthesizing PMN by solid state reaction [20]. In a temperature range of 800°C- 1000°C they successfully synthesized phase pure PMN. By introducing a precursor and a two stage synthesis route they were able to avoid the parasitic pyrochlore phase known to cause a severe reduction in the dielectric permittivity [20]. This method has later been adapted to the solid state synthesis of PSN using the so called *Wolframite method* and a $ScNbO_4$ precursor [21-23]. However, solid state synthesis requires heating at high temperatures which conflicts with ordering in PMN, but a new approach to synthesize both PMN and PSN has already been introduced. Molten salt synthesis allows nucleation and growth of both PMN and PSN in a molten salt solution [7, 24, 25]. Yoon *et al.* [25] reported successful results when synthesizing PMN at 750°C using a 0.5NaCl- 0.5KCl salt combination with a reported melting point of 650°C [24, 25]. However, no known studies have been focusing on B- cation ordering by molten salt synthesis of these materials until it was recently investigated by us [7]. The motivation was a study by Fuoco *et al.* which showed it possible to synthesize B- cation ordered Sr_2FeReO_6, Ba_2FeReO_6 and

Sr_2CrReO_6 using a 0.5NaCl-0.5KCl salt combination [26]. For this reason we believed it also possible to synthesize cation ordered PMN which has never been done. Our discoveries on molten salt synthesis of PMN and ordered PSN encouraged to continue with further experiments. We found that molten salt synthesis of PMN at 750°C for both 2 hours and 20 hours resulted in similar particle sizes, and a small degree of ordering could be observed in molten salt synthesized PSN. Molten salt synthesis of PSN using a precursor can therefore be used to observe the precursor's effect on ordering as well as the phase purity, and to this date no known studies have reported results on this topic. There were also many parameters that were not included in our earlier study, such as heating- and cooling rates which may influence the cation ordering.

1.2 Objectives

The main objective of this study is to continue on a long line of work concerning lead based ferroelectric relaxors. PSN will be investigated further to observe new parameters' effect on ordering and phase purity. Some of this will be a reproduction of earlier work. In addition, new parameters will be used in the attempt to obtain cation ordered PSN powder by molten salt synthesis. To compare with the molten salt synthesis, dense PSN pellets will be made, and dielectric spectroscopy used to study the effect of annealing on the dielectric properties.

- Synthesize ordered PSN using molten salt synthesis with and without a precursor.
- Synthesize ordered PSN by solid state synthesis and subsequent annealing.
- Investigate the annealing effect on the dielectric properties.

2. Theory

2.1 Ferroelectric perovskites

As a result of spontaneous polarization, certain materials display ferroelectric properties [1, 9, 10] . This spontaneous polarization, or charge separation, leads to a dipole moment and the origin of this dipole moment can be of different kind [1, 9]. Octahedral sites and/ or lone pair containing ions contribute to the ferroelectric properties in perovskites [1]. A well-known perovskite is $BaTiO_3$ [9] which has the atomic structure ABO_3 shown in Figure 2.1.1. Above the Curie temperature, T_C, the Ti^{4+} ions are on average located at the center of an oxygen octahedron due to thermal movement. At this point there is no dipole moment. However, when an external electric field is applied the crystal may be polarized, but when removing the field, the polarization disappears with it. Below the Curie temperature, the crystal structure stabilizes by the formation of a covalent bond between the Ti^{4+} ions and one of the six octahedral oxygen anions. This bond formation reduces the structure symmetry and causes an uneven distribution of positive and negative charges in the material which is now a dipole. The spontaneous bond formation between titanium and oxygen can be explained by the cation size differences. Because of the large Ba^{2+} ions, the oxygen octahedra dimensions are forced to change and causes an increased oxygen- titanium bond length [1]. The tolerance factor t, is usually used to describe this phenomenon [1]. $BaTiO_3$ has a tolerance factor of 1.06 at room temperature which means that the A- cation is larger than the B-cation and that a tetragonal and ferroelectric $BaTiO_3$ is expected [1]. A tolerance factor below 1, for example between 0.85 and 0.9 like for $GdFeO_3$, causes different structural distortions. In $GdFeO_3$ the BO_6 octahedra are tilted in a zigzag pattern while for t smaller than 0.85 the distorted perovskites are no longer stable and ceases to exist [1].

The Curie temperature marks the phase transition from cubic to tetragonal $BaTiO_3$ and the point at which spontaneous polarization occurs. Below the Curie temperature one of the dimensions of the cubic unit cell expands to create a c- axis while the two other axes, a and b, contracts [9]. In this tetragonal and ferroelectric state $BaTiO_3$ is able to retain a net polarization even when the external electric field has been removed. This polarization is called the remnant polarization (P_r) and is illustrated in Figure 2.1.2.

The net polarization in ferroelectric materials can be explained by ferroelectric domains [1]. Ferroelectric domains are parts of the material in which the dipoles point in the same direction. When the net polarization is zero, the dipoles point in random directions and cancel each other out. But when an external electric field is temporarily applied to $BaTiO_3$ when below the Curie temperature, the dipoles align to point in the same direction, causing a net polarization that continues to exist when the field has been removed. In $BaTiO_3$ this can be thought of as the electric field forcing the Ti^{4+} ions to bond with a certain oxygen anion.

In PbTiO$_3$, the ferroelectric properties are caused by an additional bonding. The A- cations (Pb^{2+}) are surrounded by a lone pair which forms stable PbO bonds to the octahedral oxygen anions [27]. By doing so, the movement of Pb^{2+} is coupled with the movement of the ferroelectric active Ti^{4+}. As a consequence of this coupling which extends throughout the crystal lattice, the displacement of the ferroelectric active Ti^{4+} cations are stabilized through an activation barrier as Pb^{2+} now also must move to change the polarization [27]. The effect of this stabilization is a large Curie temperature(T$_C$) of 490°C compared to 120°C for BaTiO$_3$ [1, 27]. This coupling between the ferroelectric active cation should be remembered for later theory on relaxor ferroelectrics.
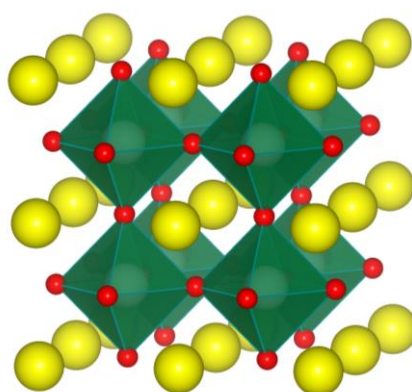

Figure 2.1.1 *Illustration of a perovskite structure ABO$_3$. A- cations, BO$_6$ octahedra and oxygen anions in yellow, green and red respectively(Made with VESTA visualization software).*

Due to the physical properties described above, ferroelectric materials are characterized by a hysteretic response to an external electric field. Figure 2.1.2 shows a typical response to an electric field with an increasing polarization of the material for an increasing field strength. From zero polarization, when the ferroelectric domains point in random directions, the polarization increases with the field until the domains point in the same direction and the polarization is said to be saturated (P$_{sat}$). Upon removal of the electric field, the material now retain a net polarization called the remnant polarization (P$_r$). To reach zero polarization, a reversed field with a strength of E$_c$, the coercive field, must now be applied. When the field strength is reduced even more, the polarization has been inverted. From the figure it can be seen that the only way to obtain zero polarization is to vary the field strength, but by heating the material to above the Curie temperature, the ferroelectric domains will again point in random directions and the net polarization will be zero without applying a field.
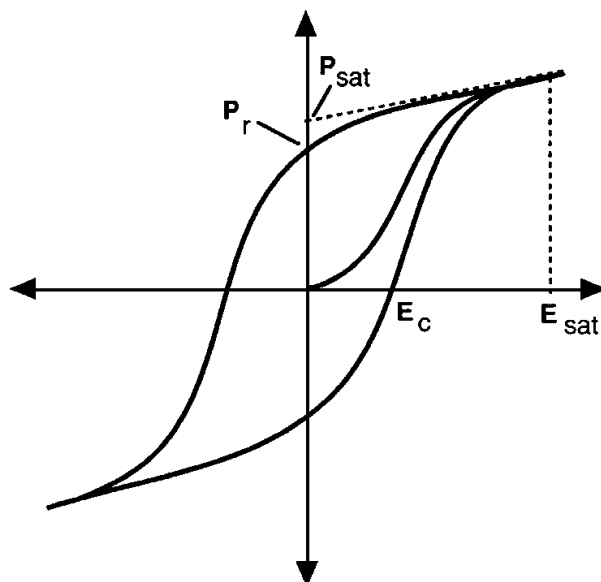
Figure 2.1.2 *Hysteresis loop for a ferroelectric material. The polarization P varies with the applied external field E up to the saturation polarization P_{sat} at the saturation field E_{sat} [6].*

Ferroelectric relaxors display larger dielectric constants which stretches over a wider temperature range when comparing with classic ferroelectrics which is illustrated in Figure 2.1.3 [3, 8, 28]. In addition, the permittivity maxima temperature is frequency dependent which can be seen in Figure 2.1.4. For increasing frequencies of an applied alternating electric field, the permittivity maxima temperature is shifted to higher temperatures. Ordered nano domains which exist to some extent in all relaxors are usually used to explain this behavior [3]. These nano sized cation ordered domains which will be discussed in detail in the next two chapters have been confirmed to have a great influence on both the magnitude and the dispersion of the dielectric constant [4]. By increasing the degree of cation ordering, the relaxor behavior is lost in some materials [23, 29] but as explained later, some materials still show relaxor behavior when ordered.
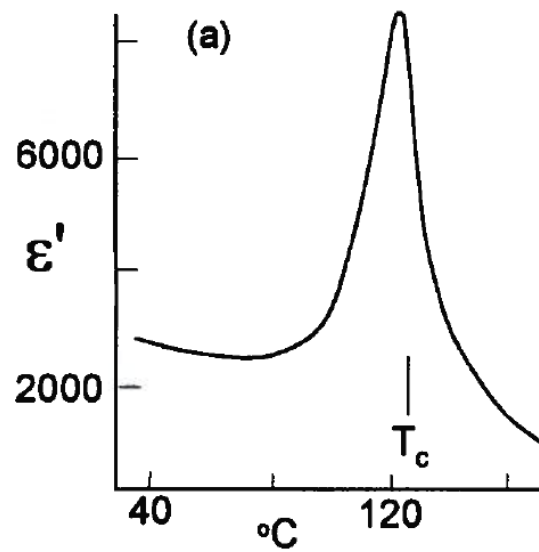
Figure 2.1.3 Dielectric response of a classic ferroelectric material, BaTiO₃, showing a large peak in the dielectric constant near T_C [1].
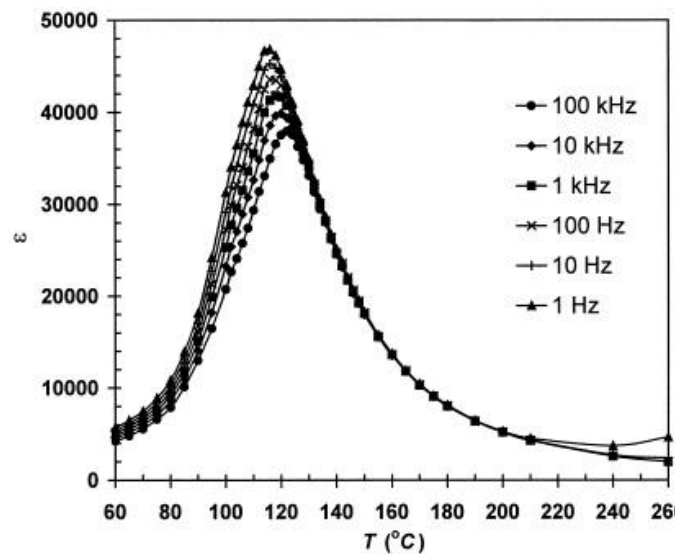
Figure 2.1.4 Temperature dependences of dielectric permittivity of 0.75PMN–0.25PT ceramics measured at different frequencies. For increasing frequencies the relaxor-ferroelectric phase transition temperature is shifted to higher temperatures and the dielectric permittivity is lowered [8].

8

2.2 Cation ordering

Perovskites can be represented as ABO_3 where A and B are cations. In relaxor perovskites the B- site is occupied by two different cations. $Pb(Mg_{1/3} Nb_{2/3})O_3$ and $Pb(Sc_{1/2} Nb_{1/2})O_3$, often referred to as only PMN and PSN, are two well-known examples of relaxor perovskites. The distribution of the B- cations in the lattice determines whether the material is ordered or disordered. PSN has an equal amount of the two B- cations, B' and B'', and therefore shows a 1:1 rock salt ordering. PMN has a 1:2 ratio of B' and B'' cations which gives PMN a different kind of ordering. The next few pages will describe ordering in both $Pb(B'_{1/3} B''_{2/3})O_3$ and $Pb(B'_{1/2} B''_{1/2})O_3$ type perovskites to establish some knowledge about the physical meaning of B- cation ordering.

Rock salt, columnar and layered ordering, which can be seen in Figure 2.2.1 – 2.2.3, are the most common types of ordering in complex perovskites, although the existence of other rare structures have been reported in literature [2, 30-32].

The coordination and charges of the B- cations may be used to explain what promotes ordering and why rock salt ordering shown in Figure 2.2.1 is the most stable structure. Figure 2.2.1 shows a distribution of B- cations which is identical with NaCl, and this kind of ordering is the most energetically favorable when it comes to charge separation. Assuming that the two B- cations were Mg^{2+} and Nb^{5+} like in PMN, rock salt ordering would be the most stable type of ordering as the highly charged Nb^{5+} - cations are located as far from each other as possible. With this distribution of cations each Mg^{2+} is surrounded by 6 Nb^{5+} and the tension between the ions is at its lowest. Shown in Figure 2.2.2 is the columnar ordering where each Nb^{5+} is surrounded by 4 Mg^{2+} and 2 Nb^{5+} while in Figure 2.2.3 the layered ordering where each Nb^{5+} is surrounded by 2 Mg^{2+} and 4 Nb^{5+} shown in Figure 2.2.3. These are both less stable structures with the layered ordering being the least stable.

The general rule for B- cation ordering considers the difference in oxidation state between the two B- cations. When the difference in charge is larger than two, order is more likely than disorder. When the charge difference is exactly two, other factors such as cation size difference and bonding preferences must be taken into account [2, 27, 30, 31].

These considerations explain merely why the rock salt structure is the most preferred over columnar and layered ordering. But little can be said about ordering in $Pb(B'_{1/3} B''_{2/3})O_3$ perovskites like PMN. To be able to do so, size differences and bonding preferences should be considered. The next section will discuss in detail the two most appreciated models for B- cation ordering in perovskites.

B-site
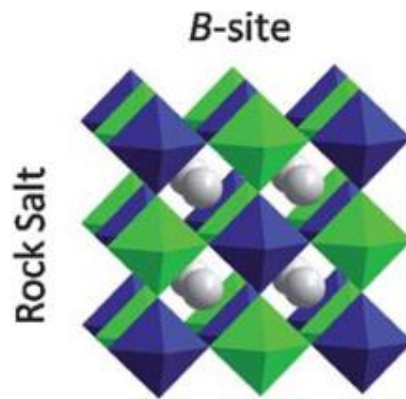
Figure 2.2.1 Rock Salt ordering of B-cations. Blue and green represents $B'O_6$ and $B''O_6$ octahedral sites [2].

Figure 2.2.2 Columnar ordering of B-cations. Blue and green represents $B'O_6$ and $B''O_6$ octahedral sites [2].

Figure 2.2.3 Layered ordering of B-cations. Blue and green represents $B'O_6$ and $B''O_6$ octahedral sites [2].

To describe ordering in complex perovskites like PMN and PSN, the most used models are the space charge model [3, 33] and the charge balanced random site model [3, 16-18]. In PMN there is a 1:2 distribution of Mg^{2+} and Nb^{5+} but the space charge model suggested that a typical PMN material would have ordering similar to $Pb(B'_{1/2} B''_{1/2})O_3$ perovskites with alternating Mg^{2+} and Nb^{5+} ions along the 100 direction shown in Figure 2.2.1 [3]. Obviously this kind of ordering implies that some kind of non- stoichiometry would have to exist. There would have to be a negatively charged ordered region and a positively charged disordered region, both of them non- stoichiometric, which was why this model was called the space charge model [3]. Studies on La- doped PMN was long used to support this model. The incentive for keeping this model was the observation of increasing 1:1 ordered domain sizes for addition of La [33-35]. The positive and negative regions thought to exist were used as an explanation for this discovery. Theory suggested that addition of La would force the ordered regions to grow in size and by that way compensate for the charge difference. A similar study on PMLT showed the same trend [17], however, later on it was shown that extended thermal treatment could increase the 1:1 order to domain sizes larger than 500nm. The 1:1 ordering in PMLT did not represent the equilibrium state of the material, but a metastable state which could be changed. This change to an almost complete 1:1 ordering was a breakthrough in the understanding of ordering as complete 1:1 order as suggested by the space charge model disagrees with the stoichiometry of PMN. Either the order had to be of a different type than 1:1 or incomplete, but they had already shown that the order was complete.

After the observation of complete 1:1 order, the space charge model could no longer be used to explain ordering. The suggested space charge model implied that the ordered materials would have to be negatively charged and non- stoichiometric, which was proven wrong by experimental results. A different model was therefore suggested, in which one of the B-sublattices is occupied by the B^{5+} ions and the other by a random distribution of B^{2+} and the rest of the B^{5+} shown in Figure 2.2.4 [3]. This model was called the charge balanced random site model as the local charge balance was maintained and large 1:1 ordered domains could be explained even in PMN. In PMN the ordering can be written $Pb(Mg_{1/2}Nb_{2/3})_{1/2}(Nb)_{1/2}O_3$ and more general $Pb(B'_{1/2}B''_{2/3})_{1/2}(B'')_{1/2}O_3$ making it obvious that ordering occurs only in one of the B-sublattices. This atomic arrangement was supported by several studies including TEM, Z- contrast imaging methods and theoretical studies of the atomic ordering in complex perovskites, including PMN [36-38].

By using Z-contrast imaging one was able to study the atomic arrangement in detail and from this explain how the space charge model could not hold [38]. From observations of intensity peaks in ordered regions of La- doped PMN the charge balanced random site model got its support. The Intensity peaks from the B' planes could be explained by a distribution of the heavier Nb- atoms in agreement with the notation above. The B' sub lattice was not only occupied by Mg- atoms but also Nb- atoms, and randomly organized. This kind of ordering differs from the rock salt ordering shown in Figure 2.2.1 where ordered planes of B'- cations alternate with ordered planes of B''- cations in the (111) direction. Instead, the blue

octahedral sites can be thought of as B^{5+} cations and on the green sites a disordered distribution of B^{5+} and B^{2+} cations. This disordered distribution of B- cations on the B'-sublattice was suggested to have a larger effect on the dielectric properties than what was earlier thought.

Davies *et al.* completed a study on ordered PMT [16] and showed that this material was still showing relaxor behavior with respect to dielectric properties. They therefore suggested that it was the random distribution on the B'- sublattice that was responsible for the frequency dependence and not the ordering between the B'- and B''- sublattices [18].
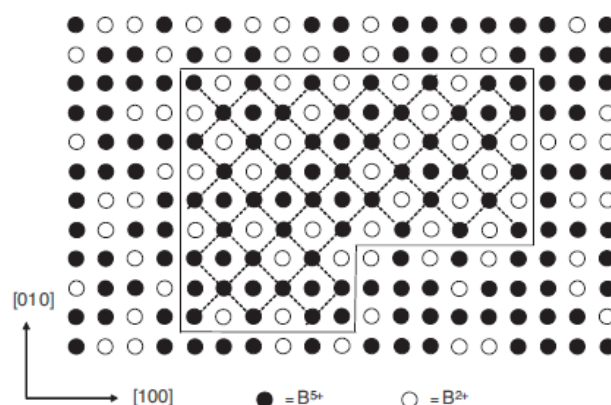

Figure 2.2.4 Illustration of the charged balanced random site model with the ordered chemical Nano region outlined. Black and white dots represent B^{5+} and B^{2+} cations respectively [3].

To be able to explain ordering and to predict the synthesis conditions needed, Daviet *et al.* developed a model [18]. By considering the sizes and charges of the B- cations they could calculate the configurational entropy of disordered and ordered PMN-PSN combinations to obtain the difference between them, which is the entropy of ordering ΔS_{ord}. By using experimentally found order- disorder temperatures they could calculate the enthalpy of ordering from $T_{dis}\Delta S_{ord}$ because at T_{dis} the Gibbs free energy is zero which means that $T_{dis}\Delta S_{ord}$ = ΔH_{ord}. At this point there is no driving force favoring either the ordered or disordered structure, but they are equally favored with respect to thermodynamics [18]. What they found was a close to linear relationship between the amount of scandium substituted and the enthalpy of ordering, from pure PMN (-3835J/mole) to pure PSN (-8542 J/mole). This means that over the double amount of energy has to be put into the system to enter the disordered region when comparing PSN to PMN. But there is of course also the entropy contribution.

In their calculations they assume that xSc^{3+} is substituted with $(2x/3)Mg^{2+} + (x/3)Nb^{5+}$ on the disordered B' site [18]. This substitution maintain the average charge on the B' and B'' sub lattices which will still be +3 and +5. However, when looking at the sizes of the B- cations, the substitution causes an average size increase on the B' site from $[(2r/3)Mg^{2+} + (r/3)Nb^{5+}]=$ 0.693 Å to $(r(Sc^{3+}) = 0.745$ Å [18]. When comparing with $(r(Nb^{5+}) = 0.64$ Å it can be seen that the substitution of PSN into PMN causes an increase in size difference between the B' and B'' sub lattices. However, there is one more effect that stabilizes ordering. The large difference in enthalpy of ordering could not be explained by the size differences between the B' and B'' sub lattices alone. The size and charge differences on the B' site itself also contributes to the enthalpy of ordering. This is more obvious when looking at pure PMN. In that case there are only Mg^{2+} and Nb^{5+} present on the B' site. This maximizes the charge and size difference on the B' site. When now looking at substitution of PSN into PMN this can be thought of as a reduction of B' site stability. The reason for this is the charge difference between the ions on the B' site which decreases for increasing scandium substitution. The average charge is still +3 as mentioned above, but the more positively charged scandium atoms reduces the charge difference on the B' site. At the same time, the scandium substitution causes a size difference increase between the B' and B'' sub lattices favoring B- cation ordering between the two of them. When considering both these effects, the large difference in enthalpy of ordering between PMN and PSN could be explained. They also found that the highest order-disorder temperature was located at 1376°C for 50% PSN substitution which is a compromise between the composition with the highest enthalpy stability (PSN) and the least negative entropy of ordering (PMN). All the theory on stability on the B' site is also supported by the theory on ordering by King and Woodward [2].
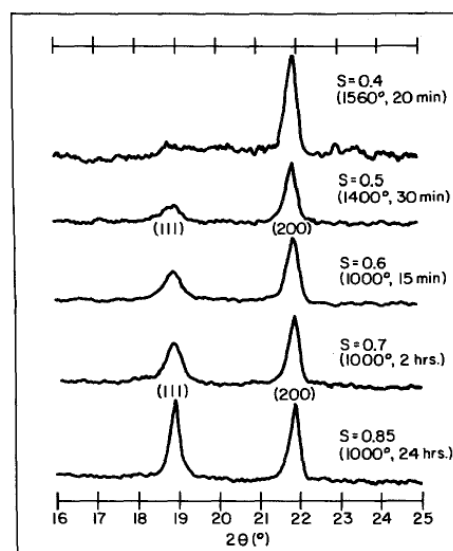
Figure 2.2.4 XRD powder diffraction pattern of PST with different degrees of B-cation ordering. Largest degree of B-cation ordering at the bottom [4].

The theory on stability of the rock salt structure may also explain the difference in lattice constant values between an ordered and disordered crystal structure. Figure 2.2.4 above by Setter *et al*. shows PST with different degrees of cation ordering [4]. The cation ordered structure (S.G. 225, Fm-3m) displays super reflections at certain angles which are correlated to the distance between the ordered (111) planes. In PST and PSN, one of these reflections can be found at $2\theta \approx 18.4°$ [39] and $2\theta \approx 18.8°$ [7] respectively. Table 2.2.1 below lists lattice constants for both ordered and disordered PSN and PST. For both PST and PSN, the ordered structure displays lattice constants in the lower range of reported values, which may be explained by the reduced repulsion in a rock salt ordering as explained above. In addition, the larger scandium ions are now surrounded by the smaller niobium ions and vice versa.

Table 2.2.1 Lattice constants of ordered and disordered PST and PSN found in literature and from own experimental studies.

Perovskite	$a_{disordered}$	$a_{ordered}$[1]
$Pb(Sc_{1/2}Nb_{1/2})O_3$ (PSN)	4.074Å [39] $-$ 4.086Å[40]	4.075Å[2] [7]
$Pb(Sc_{1/2}Ta_{1/2})O_3$ (PST)	4.072Å [41] - 4.080Å [40]	4.068Å [39]

1. Half of the superstructure (S.G. 225, Fm-3m) lattice constant. 2. Small degree of ordering.

2.3 Cation ordering effect on dielectric properties

As mentioned in the previous chapters, ordering can have a great impact on the dielectric properties of relaxors. To understand why, the true nature of relaxors should be paid attention to. All relaxors contains small domains of different size which below a certain temperature T_B, are polar and dynamic [3]. These domains, often referred to as polar nano regions (PNR) are believed to cause the frequency dependence of the permittivity maxima temperature T_m. The PNR are ordered with respect to the B- cations due to the alternating B' and B'' cations in the (100) direction. Second, cation ordering due to thermal annealing is somewhat a misleading phrase as ordering is already there to some extent. The cation ordering, as confirmed by several studies, is rather growth of already existing ordered domains [18, 42].

Different suggestions to the relaxor behavior can be found in the literature but most common are two descriptions [3, 43, 44]. Based on these, Cheng *et al.* have developed a mathematical model that describes the dielectric response [45, 46]. Two mechanisms, one above and one below T_m are commonly believed to be responsible for the dielectric behavior. At higher temperatures, the PNR are polar and dynamic and the dielectric properties are governed by flipping of the polar domains. The alternating electric field causes the PNR to flip when the temperature is high enough. Upon cooling however, both the number and size of PNR increases and causes them to freeze. The reason for this is the increasing interactions between them [44]. The consequence of this is an increasing relaxation time, i.e. the time for the PNR to reorient, and thus at high frequencies and lower temperatures, the alternating field frequency is too high for the relaxation, thus a shift in T_m will occur. That is, the dielectric maxima occurs at different temperatures for different frequencies. At high frequencies, higher temperatures are needed for reorientation of the PNR to be possible. The freezing of PNR has also been used to explain how frequency dependence is lost upon ordering [29]. For increasing degree of ordering, the number and size of the PNR increases fast upon cooling below T_B. The increasing number and size of PNR also increases interactions between them, and on complete ordering, the PNR are all coupled and frozen. At this point, there is no reorientation of the PNR and polarization independent of frequency. The mechanism believed to govern this state is referred to as the breathing model [43].

Below T_m (for relaxors) or upon complete ordering (PSN) the PNR are believed to be more or less frozen and pinned by elastic and electrostatic forces [29, 43]. The effect below T_m is referred to as breathing of the PNR and was developed by Glazounov and Tagantsev [43]. This is described as sideways motion of the PNR boundaries without any reorientation when exposed to an external electric field. However, when the PNR are moving, the volume changes and therefore the polarization.

Increasing degree of cation ordering has also been shown to reduce the permittivity maxima temperature (T_m) and dielectric permittivity (ε_m) [29]. Also, the same way as Pb^{2+} has shown its importance in raising T_C in $PbTiO_3$ [1, 27], an A- site substitution or vacancy has been

shown equally important in reducing T_m in PSN and other relaxors [22, 27]. A relationship has been found between A- cation displacement and T_m, where T_m is proportional to d_{Pb}^2 with d_{Pb} being the average Pb displacement from the ferroelectric active Nb^{5+} cation [47, 48]. In ordered PSN, the Pb^{2+} cations will move towards the larger B'- cation [27]. The reason for this is the larger Sc^{3+} cations pushing the intermediate oxygen ions outwards. Also, the intermediate anions around Nb^{5+} are distorted towards the Nb^{5+} cations away from Pb^{2+}. As a consequence, the Pb^{2+} forms stable PbO bonds with the oxygen anions in the ScO_6 octahedra. The coupling between the Nb^{5+} and Pb^{2+} is this way lost, hence the reduced T_m. In a disordered PSN however, the Pb^{2+} and Nb^{5+} are coupled through a repulsion which distorts the Pb^{2+} cation. Of the two scenarios, d_{Pb} is here largest [27, 48], and according to the relationship above, T_m will be large. Or analogous to $PbTiO_3$ situation, the stabilization will be large and hence a larger T_m.

2.4 Molten salt synthesis and cation order- disorder

Molten salt synthesis (MSS) is a synthesis method typically used to synthesize ceramic powders at lower temperatures than what would otherwise be necessary when using conventional solid state synthesis [24, 25]. In molten salt synthesis a salt combination e.g. 0.5NaCl-0.5KCl is mixed with the reactants to lower the barrier for product particle formation. The molten salt synthesis has also been shown as effective in controlling particle shapes and sizes by varying the amount of salt [7]. Among other effects, wetting between reacting particles typically leads to an increasing driving force for particle formation by increasing the pressure at contact sites. As described by Kimura *et al.* [24] there are several possibilities for particle formation in the liquid salt. Among them, heterogeneous and homogenous nucleation. When the salt/reactants mixture is heated to high enough temperatures so that there is only dissolved reactants/particles in the liquid, then and only then can homogenous nucleation occur. Homogenous nucleation means that the product particles are formed somewhere in the liquid, while for heterogeneous nucleation the product particles are formed by nucleation on particles that have not been dissolved in the liquid salt. Also mentioned by Kimura, is the fact that after a homogenous nucleation, there are still reactants dissolved in the liquid salt and upon cooling product particles may form on the existing product particles. This can be described as an initial homogenous nucleation followed by heterogeneous nucleation. For single crystal growth, homogeneous nucleation is achieved by complete dissolution of reactants, and by varying the cooling rate, the number of nuclei formed can be controlled [49]. When large single crystals are wanted, the number of nuclei should be at a minimum. However, for molten salt synthesis of ceramic powders, a large number of nuclei and product particles are usually preferred, and therefore complete dissolution of reactants is not necessary. The larger number of nuclei formed reduces the final particle sizes which is an advantage when the powder will be used for sintering dense materials.

The advantages with molten salt synthesis can be summarized with lower synthesis temperatures and the possibility of controlling the growth. The increased reaction rates can be attributed to an increased diffusivity and mobility of reacting particles as well as increased contact pressure between particles, the latter effect resulting in an increased solution and precipitation can be seen in liquid phase sintering [10]. The downside of using a molten salt is that the reactants may react with the salt resulting in unwanted byproducts [7]. Important is also that the salt should easily wash away by simple steps. This is normally done using heated deionized water for NaCl, KCl and combinations of these [24, 25].

As mentioned in the previous chapter, the models developed by Davies *et al.* [18] can be used to explain the synthesis conditions needed to obtain cation ordering. From Figure 2.3.1 below, the order- disorder temperatures for PMN and PSN combinations can be seen. Ordered PMN, from a thermodynamic point of view, must be annealed below approximately 940°C to obtain ordering. For PSN, this temperature is approximately 1210°C.
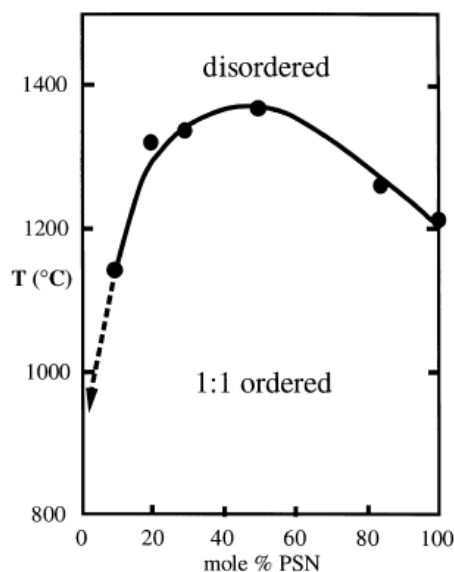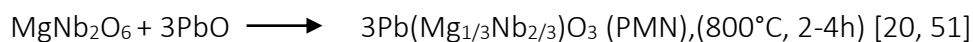
Figure 2.3.1 *Order- disorder temperatures for the PMN- PSN system. Hatched line indicates extrapolation to pure PMN* [5].

However, it is not only the order- disorder temperature that should be considered when synthesizing these materials. There is also a lower temperature limit for ordering to take place within reasonable time in solid state synthesis. This temperature limit and above, called the kinetically active region by Davies *et al.,* indicates the region where the cation mobility is high enough for ordering to take place [18]. They suggested that this temperature was located around 1070°C. It should though be noted that other studies show that annealing PSN at 940°C- 1000°C is sufficient to obtain cation ordering [29, 42]. However, when looking at the left end of the diagram in Figure 2.3.1 and other studies by Davies and Akbas [5, 18, 50], the order- disorder temperature is suggested to lie maybe as low as 900°C- 950°C. From the facts above, it can be concluded that a different approach must be made to obtain cation ordering in PMN as annealing below 900°C means annealing below the active region. Therefore in an attempt to make ordered PMN, molten salt synthesis was recently investigated as a possible route due to the benefits mentioned in the beginning of this chapter [7]. Although high purity PMN could be made, no cation ordering was observed even though synthesis was carried out below the order- disorder temperature. However, the same study revealed a small degree of cation ordering in molten salt synthesized PSN. Even though long range order has been obtained in PSN before, there is significant annealing time related to ordering PSN, and time and energy consumption reduction is always beneficial. Molten salt synthesis is therefore one possible solution to this problem.

Although solid state synthesis can be used to make both PSN and PMN [42, 51], previous work show that the temperatures needed to obtain high purity PMN is significantly higher when compared to molten salt synthesis [7]. At 750°C for 2 hours high purity PMN was made, but for solid state synthesized PMN, three times grounding and calcination at 850°C for 2 hours was still not enough. In solid state synthesis the powder is usually compacted into pellets to increase contact between particles. This is obviously a step that is not needed for molten salt synthesis as the powder mixture is poured into a crucible and heated. For solid state synthesis the grounding, calcination and pressing is usually repeated several times before the reaction is complete, which in most cases is due to the limited cation mobility compared to molten salt synthesis. The higher temperatures required in solid state synthesis may also cause evaporation of volatile compounds such as PbO. Therefore, to maintain stoichiometry and reduce evaporation from the surface, sacrificial powder [5] and PbO excess [42] is typically used.
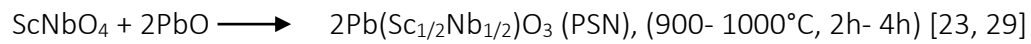
In 1982, in an attempt to reduce the amount of pyrochlore ($Pb_2Nb_2O_7$ etc.) when synthesizing PMN, Swartz *et al.* developed a two stage process involving a precursor [20]. The pyrochlore phases are unwanted because of their damaging effect on the dielectric properties. Compared to PMN, the pyrochlore phases have a 100 times smaller dielectric constant which means only small amounts are needed to have a large effect [51]. By introducing this precursor, they were able to make phase pure PMN and according to Swartz *et al.* there were two important reasons for the success. The splitting of the $MgNb_2O_6$ to Nb_2O_5 and MgO was assumed to be slower than the reaction between the precursor and PbO. In addition, the *Columbite* structure is an oxygen octahedra structure similar to the perovskite structure. The parasitic pyrochlore could therefore be prevented by following the steps below.

$$MgO + Nb_2O_5 \longrightarrow MgNb_2O_6 \text{ (\textit{Columbite}), (1000C, 6h)}$$

$$MgNb_2O_6 + 3PbO \longrightarrow 3Pb(Mg_{1/3}Nb_{2/3})O_3 \text{ (PMN),(800°C, 2-4h) [20, 51]}$$

Heterogeneous nucleation described above means particle formation on some other particle. When molten salt synthesizing PMN using a precursor, the possible nucleation sites are this way reduced to one compound. Otherwise, MgO and Nb_2O_5 could both function as nucleation sites as they are the least soluble compounds in this case [25]. This theory may be used to explain the successful results in the previous study [7].

Both solid state synthesis and molten salt synthesis show successful results when using a precursor. However, the recent study, which included synthesis of both PMN and PSN did not include a precursor to synthesize PSN.

Several studies report successful results using a $ScNbO_4$ precursor to make phase pure PSN through the so called *Wolframite method* [22, 23, 29, 52]. By first making a precursor and then mixing the precursor with lead oxide, phase pure PSN is easier to obtain. The reaction routes and parameters commonly used for solid state synthesis are shown below.

$Sc_2O_3 + Nb_2O_5 \longrightarrow 2ScNbO_4$ (*Wolframite*), (1250°C, 4h)

$ScNbO_4 + 2PbO \longrightarrow 2Pb(Sc_{1/2}Nb_{1/2})O_3$ (PSN), (900- 1000°C, 2h- 4h) [23, 29]

2.5 Solid state sintering

As mentioned in the previous chapter, PbO excess helps maintaining the stoichiometry, but it also works as a sintering aid. By increasing the contact pressure between the particles, the result is an increased solution precipitation rate [10]. There are also other factors affecting sintering and the resulting density of a sintered pellet. The degree of agglomeration, particle size and shape, and particle size distribution are among the most important [10].

Smaller particle sizes are advantageous due to the faster sintering rates. The reason for this is the larger radius of curvature which results in increased contact pressure between particles. This is important both for solid- and liquid phase sintering. In liquid phase sintering, the smaller particle sizes results in an increased capillary pressure which increases the contact pressure between particles.

Excess PbO has been shown to have a great effect on sintering [53]. The sintering rates are to some extent dependent on the amount of excess PbO, causing either coarsening or sintering for low and high PbO content respectively.

Agglomeration causes non uniform particles which reduces the driving force for sintering. Also, long and flat particles generally have a smaller driving force for sintering which is related to the radius of curvature mentioned above. Some particles may even have a negative radius of curvature which reduces the driving force for sintering significantly. A consequence of such particles are typically irregularly shaped pore sizes which are difficult to remove.

Particle size distribution also plays an important role for particle sizes of micrometer size. A narrow distribution reduces the compacting during pressing and often results in large pores after sintering.

3. Experimental

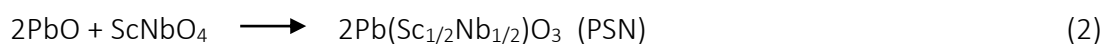## 3.1 Solid state synthesis of PSN (*Wolframite method*)

Calcination

PbO (99.999%, Sigma Aldrich), Nb_2O_5 (99.99%, Sigma Aldrich) and Sc_2O_3 (99.999%, Fisher Scientific) were dried in a vacuum furnace at 200°C overnight. Sc_2O_3 and Nb_2O_5 were then weighed, mixed in a stoichiometric amount using a mortar and compacted into a pellet of 20mm diameter using a two way uniaxial press at 47MPa. The pellet was then heated in a covered alumina crucible at 1200°C for 6 hours in a *Nabertherm P330/P320* oven to make a $ScNbO_4$ precursor through reaction 1 shown below. The grounding and calcination steps were repeated until the reaction was complete. To increase the rate of reaction 2 below, the precursor was ball milled using a *Retsch PM 100* planetary mill at 400rpm for 30 minutes (with a 50ml steel crucible and 8 balls of 10mm diameter) to reduce the particle size. To ease the powder crushing, the powder was mixed with ethanol to form a slurry which was dried prior to the PSN synthesis. PSN was then made by mixing the $ScNbO_4$ precursor and PbO in a stoichiometric amount. The powder mixture was then pressed into pellets of 20mm diameter at 23MPa pressure. The pellets were then heated in a *Nabertherm* P330 oven at 900°C for 6 hours (Batch A) and at 1000°C for 3 hours (Batch B) to obtain PSN through reaction 2 shown below. To reduce PbO evaporation, two alumina crucibles were used, and the pellets were covered with PSN powder. The outer crucible was filled with PbO powder to increase the vapor pressure of PbO outside the inner crucible. A schematic illustration of the setup is given in Figure 3.1.1. The parameters used to synthesize PSN by the *Wolframite method* are summarized in Table 3.1.1 below.
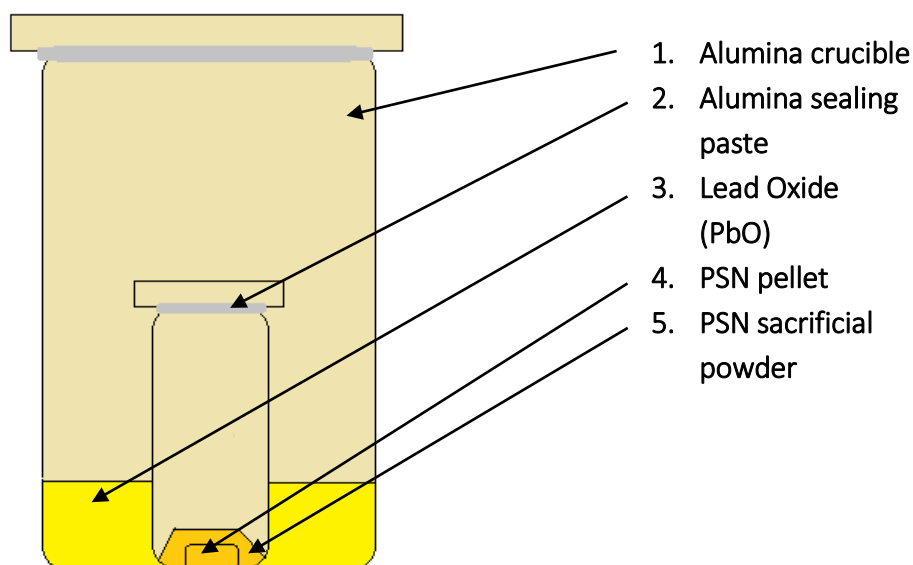
Table 3.1.1 Synthesis parameters used to prepare $ScNbO_4$ and $Pb(Sc_{1/2}Nb_{1/2})O_3$ (PSN) by solid state synthesis.

Batch	Reactants	Product	Temperature	Time	Heating rate[1]
	Sc_2O_3, Nb_2O_5	$ScNbO_4$	1200°C	6 hours	300°C/hour
A	$ScNbO_4$, PbO	$Pb(Sc_{1/2}Nb_{1/2})O_3$	900°C	6 hours	300°C/hour
B	$ScNbO_4$, PbO	$Pb(Sc_{1/2}Nb_{1/2})O_3$	1000°C	3 hours	300°C/hour

1. Oven set to cool naturally (cooling time: 0:00)

Wolframite method:

$$Sc_2O_3 + Nb_2O_5 \longrightarrow 2ScNbO_4 \tag{1}$$

$$2PbO + ScNbO_4 \longrightarrow 2Pb(Sc_{1/2}Nb_{1/2})O_3 \; (PSN) \tag{2}$$

1. Alumina crucible
2. Alumina sealing paste
3. Lead Oxide (PbO)
4. PSN pellet
5. PSN sacrificial powder

Figure 3.1.1 *Schematic illustration of the setup used to reduce PbO evaporation when synthesizing PSN.*

Sintering and annealing of PSN

PSN and different amounts PbO excess was both dry and wet (ethanol) mixed to obtain dense sintered PSN pellets. Pellets comprising of planetary milled PSN and PbO were tested along with powder that had not been milled. The pellets were all pressed with a uniaxial press of 10mm diameter, and the ideal pressure of 47MPa was found by testing. In an attempt to increase the final pellet density, some pellets were additionally pressed using an *Autoclave Engineers* Cold Isostatic Press (CIP) at 2KBar. The pellets were sintered for 1 hour at 1250°C (300°C/h) and the final samples (1-3) were sintered in the same crucible placed on top of each other separated by PSN powder. There were some difference in thickness of the pressed samples with sample1 being the thinnest while Sample2 and Sample3 had similar thickness. The pellets were also annealed for 42 hours at 1000°C (Sample1), 18 hours at 1100°C (Sample2) and for 18 hours at 1150°C (Sample3) to obtain B-cation ordering. Sintering and annealing was conducted in an *Entech* high temperature oven using a similar setup to Figure 3.1.1 without PbO in the outer crucible. The densities of both sintered and annealed pellets were measured using Archimedes method. The parameters used for sintering and annealing are given in Table 3.1.2 below.

Table 3.1.2 *Sintering and annealing parameters used to make dense PSN pellets used for dielectric measurements.*

| Sample	Sintering T/t	Annealing T/t	Uniaxial press	Cold Isostatic Press
Sample1	1250°C/1hour	1000°C, 42h	47MPa	2KBar
Sample2	1250°C/1hour	1100°C/18h, 100h	47MPa	2KBar
Sample3	1250°C/1hour	1150°C/18h	47MPa	2KBar

3.2 Dielectric spectroscopy

Preparation of pellets

Prior to the dielectric measurements, the sintered and annealed pellets had to be thoroughly polished to obtain flat and parallel surfaces. SiC paper P#800 was used with a *Struers Labopol-21* polishing table. After polishing, the pellets were rinsed in ethanol in an ultrasonic bath (*Branson 5510*) for 30 minutes and then dried for 30 minutes at 100°C. Both sides of the pellets were then sprayed with silver to function as electrodes. To avoid contact between the electrodes, the perimeter of the pellets were covered with tape during spraying. After resting 30 minutes in air, the pellets were placed on a curly aluminum foil in an oven holding 200°C. This was done to make sure all liquid from the silver spray evaporated. The curly aluminum foil was used to allow minimum contact between the silver coated surfaces and the substrate during heating.

Measurements

The measurements were done using a *Novotherm* temperature controller with a *Novocontrol* dielectric spectrometer and *WinDETA V5.84* software. The samples were placed between two electrodes with platinum plates separating the pellets from the instrument electrodes. The setup is shown in Figure 3.2.1 below. The samples were measured from 30°C-400°C and the frequency range from 1Hz to 1MHz. The heating rate was set to 2°C/min. This way the dielectric permittivity was measured as a function of both temperature and frequency to investigate the effect of thermal annealing on the PSN relaxor. Sample1 was measured before and after annealing while Sample2 and Sample3 were measured after annealing.
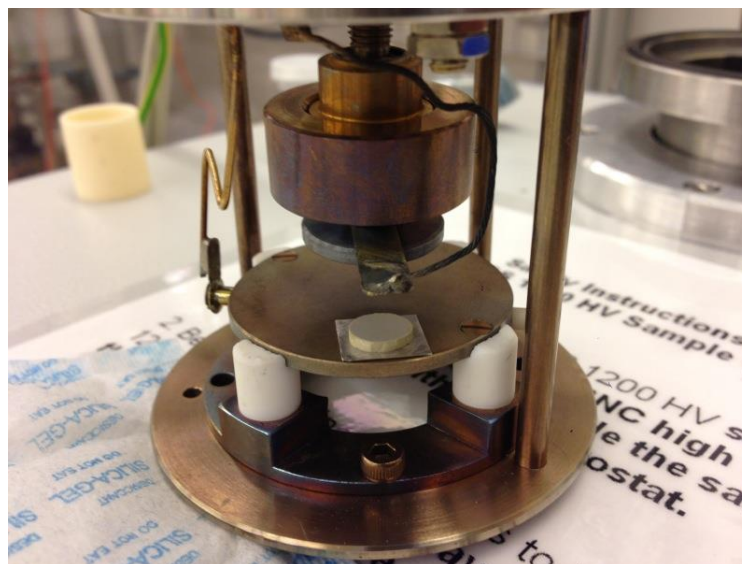
Figure 3.2.1 Image of dielectric spectroscopy setup showing the PSN pellet separated from instrument bottom electrode by a platinum plate.
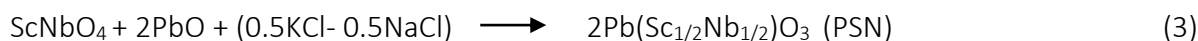
3.3 Molten salt synthesis of PSN (Route 1)

Sc_2O_3 (99.999%, Fisher Scientific), Nb_2O_5 (99.99%, Sigma Aldrich) and salts NaCl (99.99%, Alfa Aesar) and KCl (99.997%, Alfa Aesar) were dried in a vacuum furnace at 200°C overnight. Sc_2O_3 and Nb_2O_5 were then weighed, mixed in a stoichiometric amount and ground. The powder mix was then pressed into pellets of 20mm diameter at 47MPa followed by calcination at 1200°C for 6 hours in a Nabertherm P330 oven to make a $ScNbO_4$ precursor through reaction 1 from last section. The grounding and calcination steps were repeated until the reaction was complete. To make PSN, the $ScNbO_4$ precursor was then mixed with PbO in a stoichiometric amount. A 0.5NaCl- 0.5KCl salt combination was then mixed in with the oxides in a 2:1 salt to oxide weight ratio using a mortar. The mixture was then fired in a covered alumina crucible at different times and temperatures and with varying heating- and cooling rates. After heating, hot deionized water was used to wash/separate the salt from the product. The parameters used are summarized in Table 3.3.1.

Table 3.3.1 Synthesis parameters used to make $Pb(Sc_{1/2}Nb_{1/2})O_3$ (PSN) by firing a Wolframite ($ScNbO_4$) precursor and PbO in a 0.5KCl- 0.5NaCl salt.

Material	Salt to oxide ratio (wt%)	Time	Temperature (°C)	NaCl:KCl (mol%)	Heating rate (C°/h)	Cooling rate (C°/h)
PSN	2:1	2h	800	0.5:0.5	200	200
PSN	2:1	2h	900	0.5:0.5	200	200
PSN	2:1	10h	900	0.5:0.5	200	200
PSN	2:1	2h	900	0.5:0.5	200	75
PSN	2:1	2h	900	0.5:0.5	75	200
PSN	2:1	2h	900	0.5:0.5	200	Open air[1]
PSN	2:1	2h	900	0.5:0.5	Rapid[2]	200
PSN	2:1	2h	1000	0.5:0.5	200	200

1. Crucible taken out of oven at 900°C and cooled in open air on a heat conducting copper plate. 2. Crucible put into preheated oven holding 900°C.

Molten salt synthesis (Route 1):

$$ScNbO_4 + 2PbO + (0.5KCl\text{- }0.5NaCl) \longrightarrow 2Pb(Sc_{1/2}Nb_{1/2})O_3 \text{ (PSN)} \qquad (3)$$

3.4 Molten salt synthesis of PSN (Route 2)

Sc_2O_3 (99.999%, Sigma Aldrich), Nb_2O_5 (99.99%, Sigma Aldrich) and salts NaCl (99.99%, Alfa Aesar) and KCl (99.997%, Alfa Aesar) were dried in a vacuum furnace at 200°C overnight. PbO, Sc_2O_3 and Nb_2O_5 were then weighed and mixed in a stoichiometric amount. The oxides were then mixed with a 0.5NaCl-0.5KCl salt combination in a 2:1 salt to oxide weight ratio using a mortar. The mixture was then heated in a covered alumina crucible in a *Nabertherm P330* oven to make PSN through reaction 4 shown below. After heating, hot deionized water was used to wash/separate the salt from the product. The different heating times, temperatures, and heating and cooling rates are summarized in Table 3.4.1 below.

Table 3.4.1 *Synthesis parameters used to make $Pb(Sc_{1/2}Nb_{1/2})O_3$ (PSN) from PbO, Sc_2O_3 and Nb_2O_5 in a 0.5NaCl-0.5KCl salt combination.*

Product	Salt to oxide ratio (wt%)	Time	Temperature (°C)	NaCl:KCl (mol%)	Heating rate (C°/h)	Cooling rate (C°/h)
PSN	2:1	2h	800	0.5:0.5	200	200
PSN	2:1	2h	900	0.5:0.5	200	200
PSN	2:1	10h	900	0.5:0.5	200	200
PSN	2:1	2h	900	0.5:0.5	200	75
PSN	2:1	2h	900	0.5:0.5	75	200
PSN	2:1	2h	900	0.5:0.5	200	Open air[1]
PSN	2:1	2h	900	0.5:0.5	Rapid[2]	200

1. Crucible taken out of oven at 900°C and cooled in open air on a heat conducting copper plate. 2. Crucible put into preheated oven holding 900°C.

Conventional Mixed Oxides (CMO) (Route 2):

$4PbO + Sc_2O_3 + Nb_2O_5 + (0.5KCl- 0.5NaCl) \longrightarrow 4Pb(Sc_{1/2}Nb_{1/2})O_3$ (PSN)   (4)
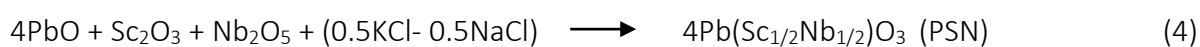
3.6 X-Ray Diffraction (XRD)

A D8 Focus was used to analyze the phase purity and crystal structure of the materials. The powders were compacted on a plastic holder and the pellets were placed on a plastic holder with a rubber. Sintered and annealed PSN pellets were polished carefully on each side using SiC paper #800 to remove the surface layer. The samples were scanned from 15° to 45° at a step length of approximately 0.2°/step and a step time of 2.0 seconds. The slit size used was 0.2mm.

A computer program *BRUKER DIFFRAC.EVA* was used to analyze the results from the scans. By using EVA, a scanned pattern can be matched to a database to detect the phases present in the sample. Each phase has a unique pattern because of the way the atoms are arranged in the crystal structure. This is used to detect not only what phases are present, but also to detect the superlattice reflections which appear when the perovskites are ordered. As explained in section 2.2, in the 1:1 arrangement of the B- cations in a rock salt structure, the B- cations are ordered so that they alternate in the (100) direction. This creates ordering of B- cations in the (111) direction. When x-rays are diffracted from the ordered crystal planes, some will then scatter from the (111) plane and this will show as intensity peaks at angles corresponding to the distance between the (111) planes.

Bruker AXS DIFFRAC.TOPAS V 4.2 was used to calculate lattice constants (a) and crystallite sizes (LVol-FWHM) by Rietveld refinement, using hkl phase and FP peak type.

3.7 Scanning Electron Microscope (SEM)

A low vacuum Hitachi S-3400N was used to characterize all produced powders by size and shape, and to study the cross section of PSN pellets. The powders were dispersed in ethanol on an aluminum stub and then coated with a thin layer of carbon using a Cressington 208Carbon. To study the pore size of the sintered pellets, they were cracked using a hammer, placed on aluminum stubs with carbon tape and carbon coated.

4. Results

4.1 Solid state synthesis of PSN (*Wolframite method*)

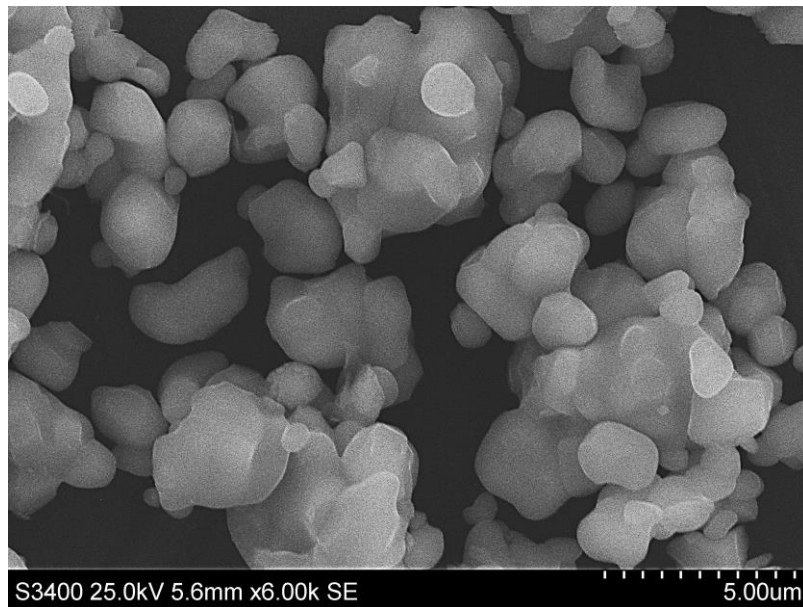### $ScNbO_4$ precursor phase purity

Figure 4.1.1 a) to c) below shows the diffraction patterns of the $ScNbO_4$ precursor used in the solid state synthesis of PSN. Diffraction pattern 4.1.1 a) below shows that the precursor had high purity after the third grounding and heating step. However small amounts of Nb_2O_5 and a non-stoichiometric scandium niobium oxide compound were observed which suggested that additional grounding and heating was needed. The powder was therefore ground and heated until the reaction was complete. Diffraction pattern 4.1.1 b) and c) shows the purity of the precursor after the 7th step and after the milling respectively. No secondary phases were detected after the 7th grounding and heating step, and the milling had no observable effects on the purity.
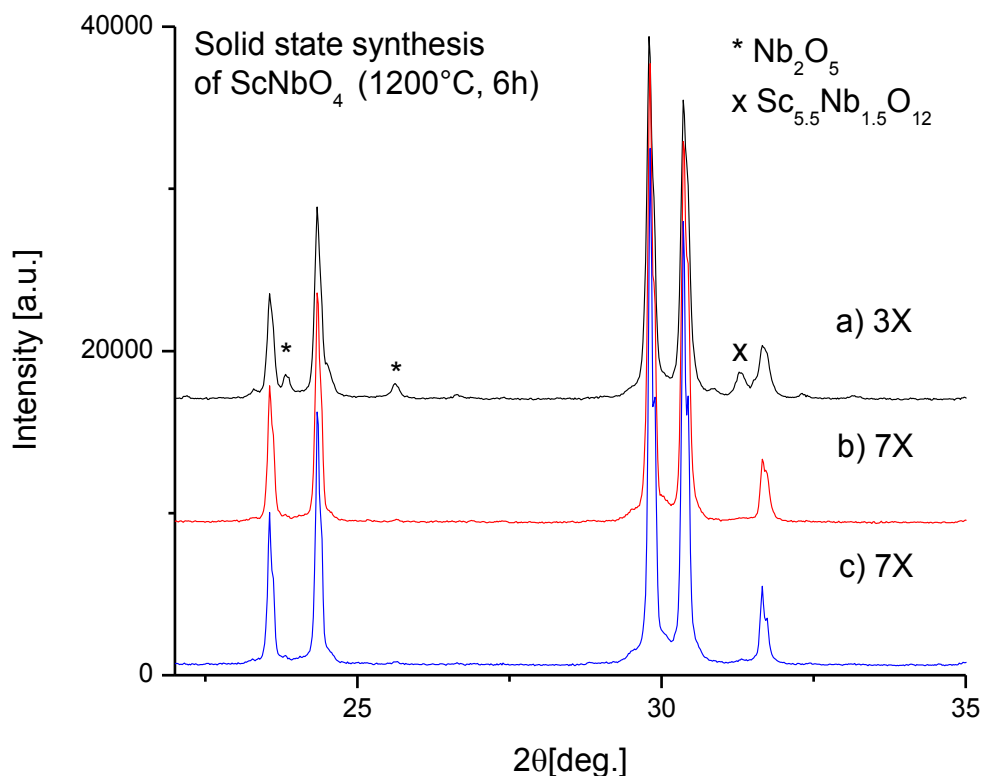
Figure 4.1.1 XRD patterns of $ScNbO_4$ precursor prepared at 1200°C for 6 hours after 3 (a) and 7 (b) times grounding and heating, and after the milling (c). Secondary phases are indicated with symbols.

ScNbO₄ precursor particle size

SEM images in Figure 4.1.2 and 4.1.3 shows the precursor particle size before and after 30 minutes planetary milling respectively. The images correspond to the diffraction patterns 4.1.1 b) and c) respectively. There was little difference in particle size before and after 30 minutes of milling. To avoid introducing impurities, the milling was therefore not continued.


Figure 4.1.2 *SEM image of ScNbO₄ precursor before ball milling.*
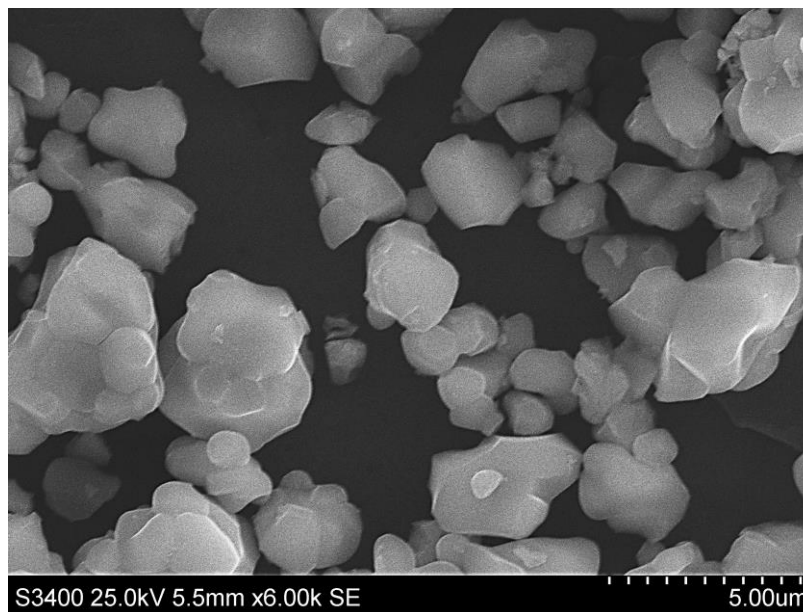
Figure 4.1.3 *SEM image of ScNbO₄ precursor after 30 minutes in Retsch planetary mill at 400rpm.*

PSN after calcination

The phase purity of PSN made using the solid state *Wolframite method* is shown in Figure 4.1.4. After the first calcination step at 900°C for 6 hours, no secondary phases could be observed. All diffraction peaks corresponded to PSN (S.G. 221 Pm-3m) and there were no indications of B- cation ordering as superreflections were not observed. The figure also shows that there were no secondary phases after milling. Batch B made at 1000°C for 3 hours was also phase pure and still no superreflections were observed at this temperature. The density of the calcined PSN pellets were roughly measured to be 40% of theoretical density. The low density could be seen as swelling of the PSN pellets. There was a visible volume increase after calcination.
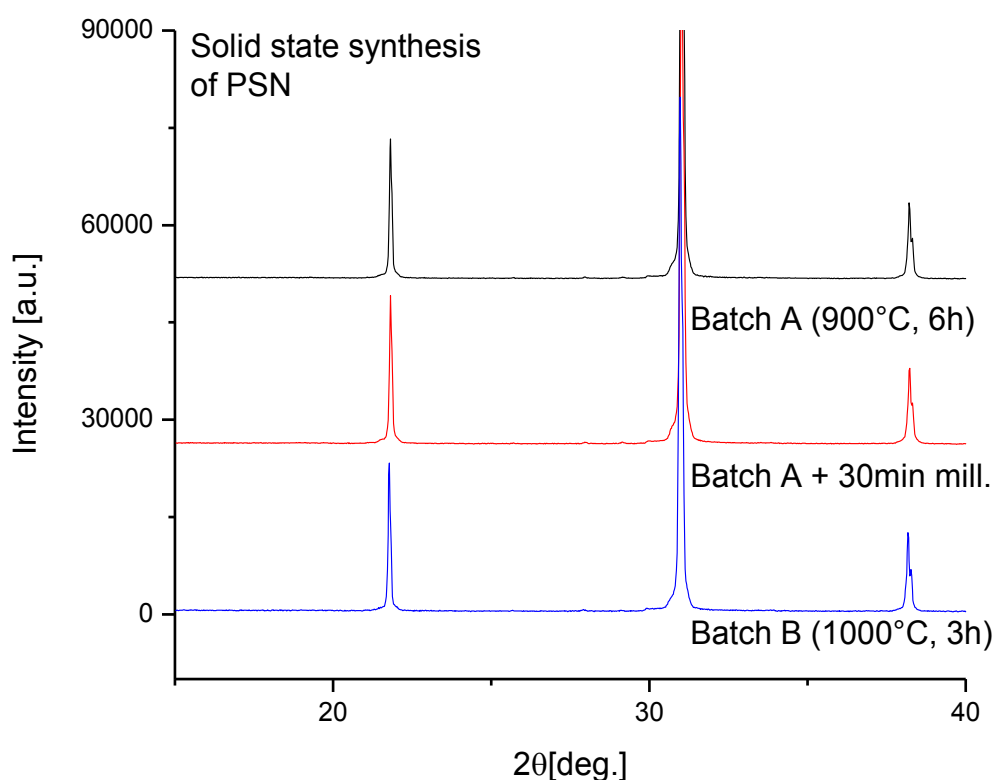
Figure 4.1.4 XRD patterns of PSN prepared at 900°C for 6 hours (Batch A) before and after milling, and Batch B made at 1000°C for 3 hours. Both batches were made using the Wolframite method with a ScNbO$_4$ precursor.

PSN (Batch A) particle size before and after milling

Figure 4.1.5 shows the particle size of the PSN powder made at 900°C for 6 hours using the *Wolframite method*. To increase the density of the sintered PSN pellets, the PSN powder was ball milled using a planetary mill. Figure 4.1.6 shows that the PSN powder particle size and agglomerates were significantly reduced after 30 minutes of ball milling at 400rpm. However, as can be seen from Table 4.1.2, the PSN particle size reduction seemed to have little effect on the final density of the sintered PSN pellets.
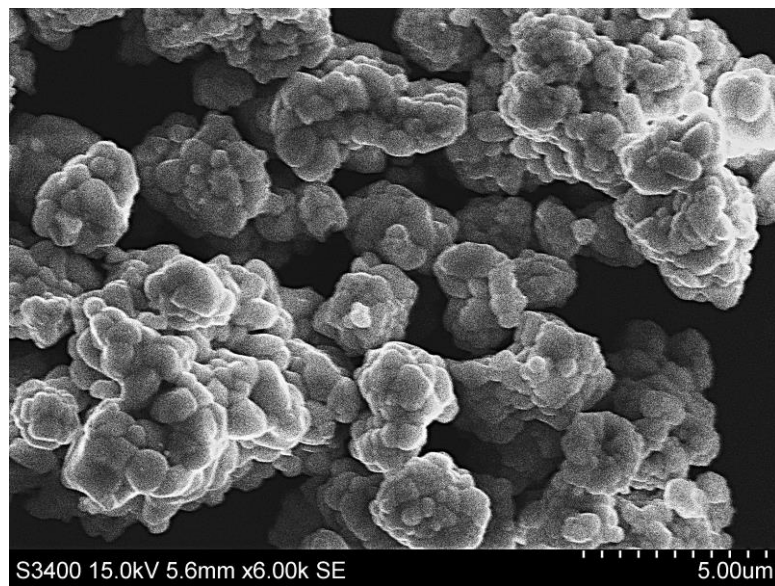
Figure 4.1.5 SEM image of PSN powder prior to ball milling.
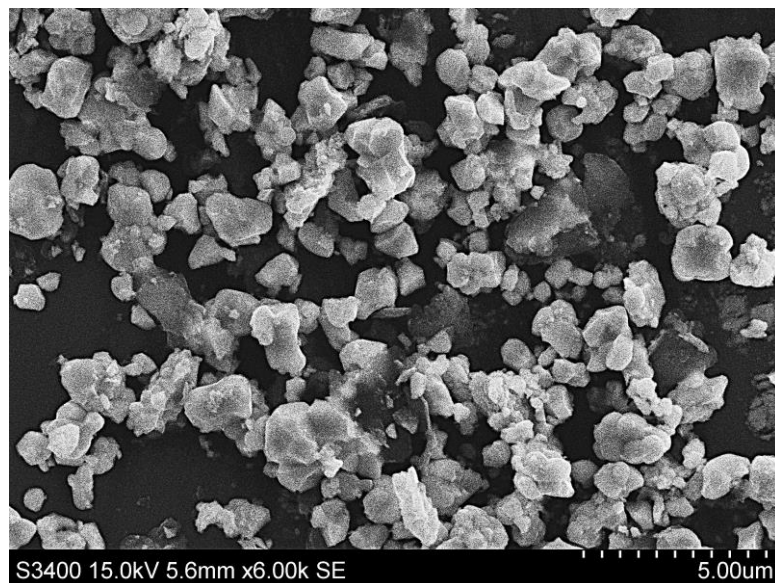
Figure 4.1.6 SEM image of PSN powder after 30 minutes ball milling.

PSN (Batch B) particle size

Figure 4.1.7 below shows that PSN synthesized at 1000°C for 3 hours gave similar particle sizes compared to batch A. However, the degree of agglomeration seemed somewhat smaller when comparing to batch A. This batch was also the one that resulted in the highest final density of the PSN pellets. Table 4.1.1 shows however that the calculated crystallite sizes were very similar and so were the lattice constants which were similar to literature values.

S3400 15.0kV 4.5mm x6.00k SE   5.00um
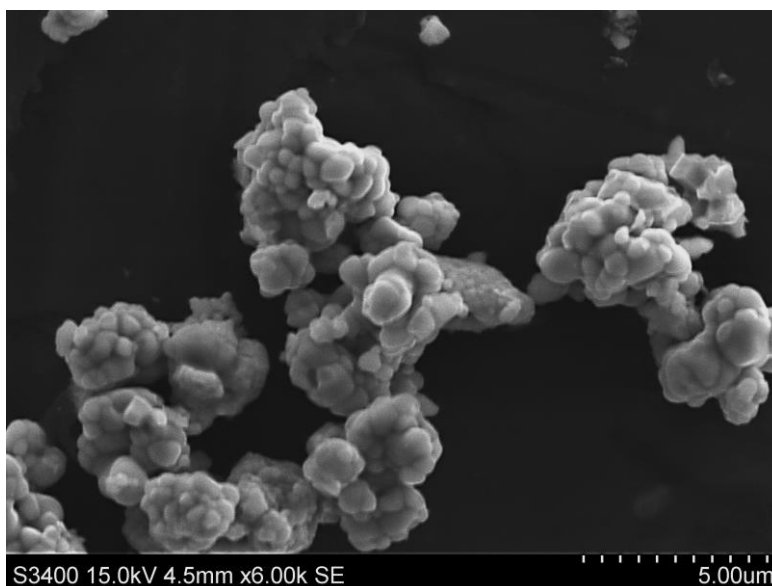
Figure 4.1.7 SEM image of PSN (Batch B) particle size synthesized at 1000°C for 3 hours.

Table 4.1.1 Average crystallite size of PSN powder after calcination from Rietveld refinement.

| Batch	Crystallite size (nm)	a (Å)[1]
Batch A	217	4.083
Batch A, milled	198	4.082
Batch B	199	4.083

1. Literature values of disordered PSN (S.G. 221, Pm-3m): (4.074Å [39] - 4.086Å [40]).

PbO particle size before and after planetary mill

Before milling, the PbO particles were quite large and irregularly shaped and the milling did have a small effect on the particle size which can be seen from Figure 4.1.8 and 4.1.9 below. However, as for the precursor, milling had little effect on the PSN pellet density.
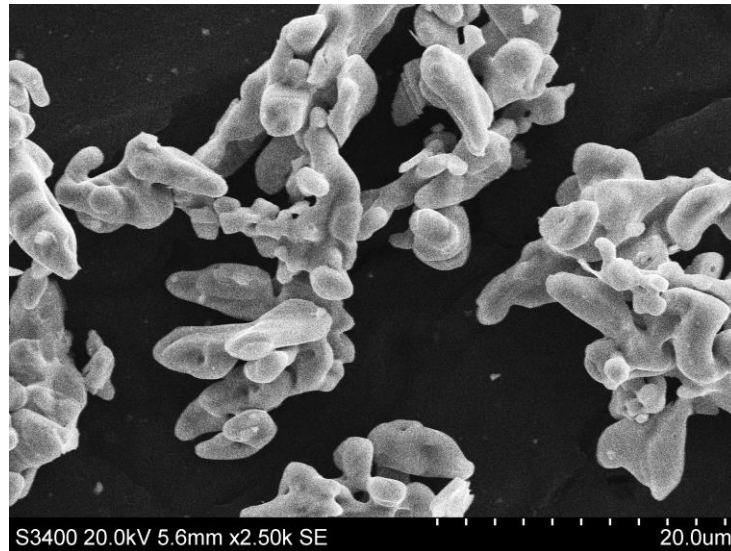
Figure 4.1.8 SEM image of PbO powder before milling.
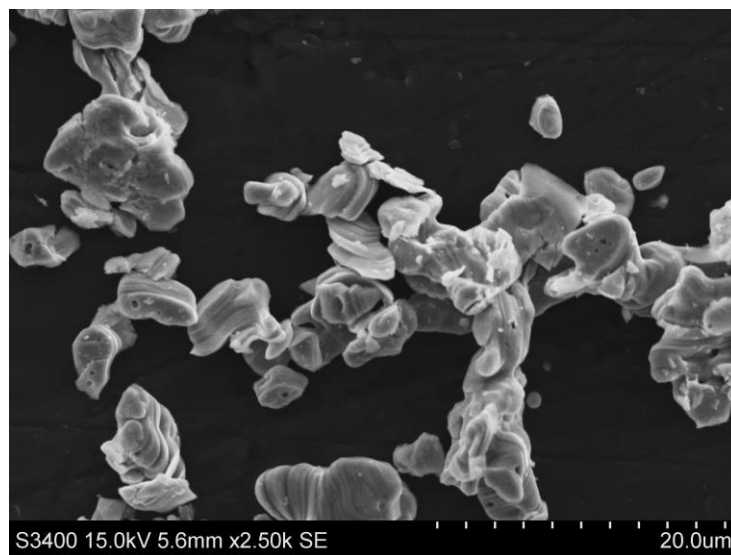
Figure 4.1.9 SEM image of PbO powder after 30 minutes in planetary mill at 400rpm.

Density of sintered PSN pellets

Table 4.1.2 shows the densities of the test samples (Test0-Test7) and the final samples (Sample1-Sample3) used for dielectric measurements. The first test sample (Test0) had a low density of 85% and high content of pyrochlore phases shown in Figure 4.1.16. But when adding a 4wt% PbO excess, the pyrochlore phases could be removed and the closed porosity decreased, but there was still a large open porosity. When comparing Test1 and Test2 it can be seen that the open porosity was reduced after 30 minutes planetary milling, and even more when wet mixing the excess PbO with milled PSN (Test3 and Test4). It should be noted that the density measurements on Test3 and Test4 were made on a piece of the pellet because they cracked during sintering. Test4 however, which was made with 8wt% PbO excess measured 92.8% of theoretical density. Test5 which was made with both milled PSN (Batch A) and 4wt% milled PbO, and wet mixed, showed a slight decrease in density to 89.4%. To investigate if this was due to voids or defects, density measurements were performed on a cracked piece as well (Test5*), but no significant difference in density could be measured. Test6 was made the same way as Test5, but in addition, the pellet was isostatically pressed. However, the increase in density was only 1.1% to 90.8%. Test7 was made with as- calcined PSN (Batch B) and 4wt% PbO, and isostatically pressed. Test7 showed a good result with little open porosity. The same parameters were therefore used to make the final samples which had similar densities as Test7 with even lower open porosity. However, Sample1 had up to 2% higher density than the two other samples.

Table 4.1.2 Calculated densities of PSN pellets sintered at 1250°C for 1 hour made with a uniaxial press 47MPa.

| Sample	PSN Batch	CIP	PbO (wt%)	Mixing	Milling (PbO)	Milling (PSN)	Open porosity	Closed porosity	Density
Test0	A	X	0	Dry	X	X	11.8%	3.2%	85.0%
Test1	A	X	4	Dry	X	X	11.1%	0.7%	88.3%
Test2	A	X	4	Dry	X	30min	6.1%	4.1%	89.8%
Test3[1]	A	X	4	Wet	X	30min	0.1%	9.0%	90.9%
Test4[1]	A	X	8	Wet	X	30min	1.5%	5.7%	92.8%
Test5	A	X	4	Wet	30min	30min	7.0%	3.6%	89.4%
Test5[1]	A	X	4	Wet	30min	30min	7.6%	2.7%	89.7%
Test6	A	2KBar	4	Wet	30min	30min	1.4%	7.8%	90.8%
Test7	B	2KBar	4	Wet	X	X	2.3%	5.5%	92.2%
Sample1	B	2KBar	4	Wet	X	X	0.3%	5.2%	94.5%
Sample2	B	2KBar	4	Wet	X	X	0.3%	7.0%	92.7%
Sample3	B	2KBar	4	Wet	X	X	0.3%	7.2%	92.5%

1. Cracked piece of pellet. Test3 and Test4 cracked during sintering.

Pore size and purity of test samples

SEM images of the cross section of pellets Test1 to Test 7 can be seen in Figures 4.1.10-4.1.17. Test1, Test2 and Test3 showed large dense areas but also a lot of irregularly shaped pores. Test4 made with 8wt% PbO excess showed the largest pore size but also large areas of high density which agrees with the measured density of 92.8%. Test5 appeared similar to Test1-Test3, but Test6 and Test7 showed somewhat larger dense areas. However, Figure 4.1.15 shows that some areas in test6, close to the perimeter, were not as dense. Except from Test4, the pore sizes were very similar and all of them had irregularly shapes pores to some extent.
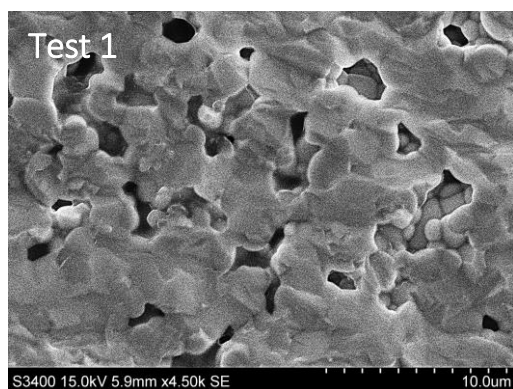
Figure 4.1.10 SEM image of cross section of PSN pellet sintered at 1250°C for 1 hour with a 4wt% PbO excess dry mixed (Test1).
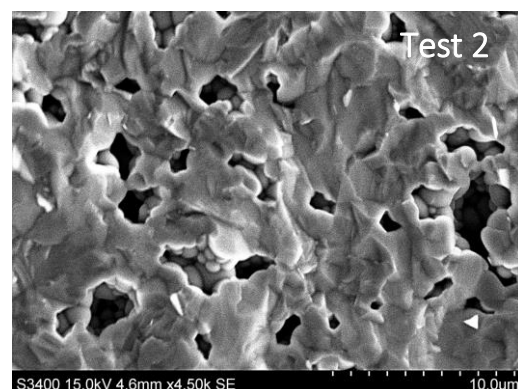
Figure 4.1.12. SEM image of cross section of PSN pellet sintered at 1250°C for 1 hour with a 4wt% PbO excess dry mixed with planetary milled (30min) PSN powder (Test2).
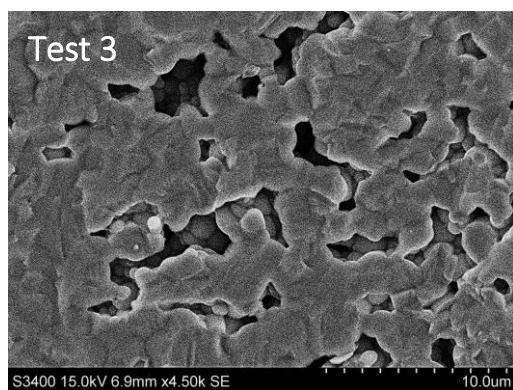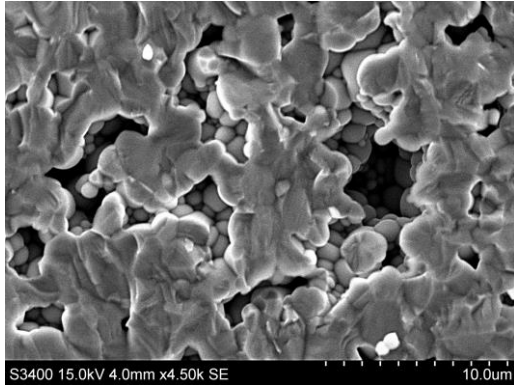

Figure 4.1.11 SEM image of cross section of PSN pellet sintered at 1250°C for 1 hour with a 4wt% PbO excess wet mixed with planetary milled (30min) PSN powder (Test3).
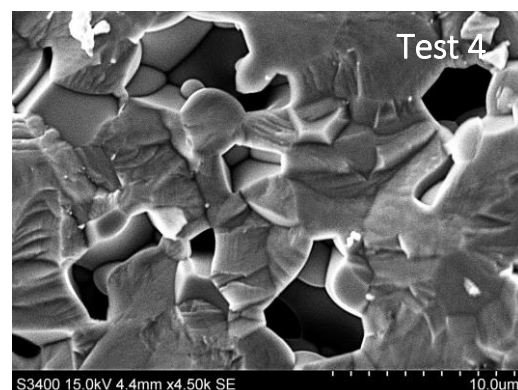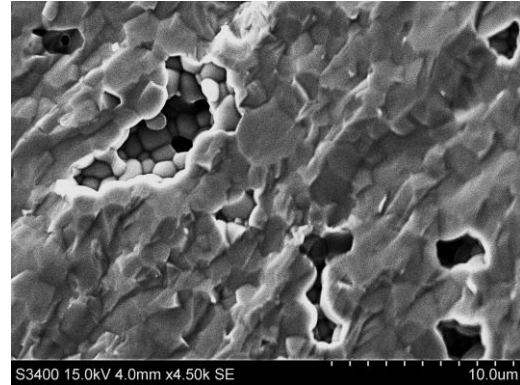

Figure 4.1.13 SEM image of cross section of PSN pellet sintered at 1250°C for 1 hour with an 8wt% PbO excess wet mixed with planetary milled (30min) PSN powder (Test4).
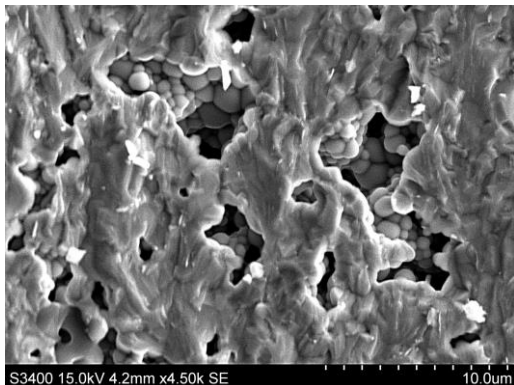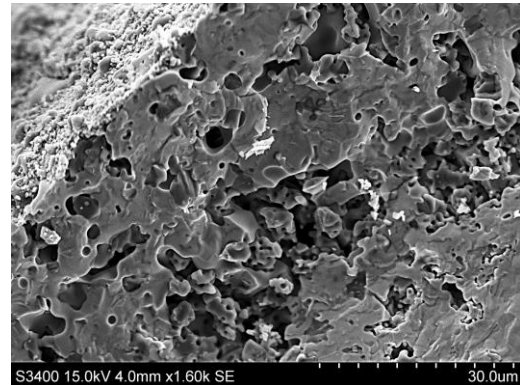
Figure 4.1.14 SEM image of cross section of PSN pellet sintered at 1250°C for 1 hour with a 4wt% planetary milled (30min) PbO excess wet mixed with planetary milled (30min) PSN powder (Test5).

Figure 4.1.16 SEM image of cross section of PSN pellet sintered at 1250°C for 1 hour with a 4wt% planetary milled (30min) PbO excess wet mixed with planetary milled (30min) PSN powder and isostatically pressed (Test6).


Figure 4.1.15 SEM image of cross section of PSN pellet sintered at 1250°C for 1 hour with a 4wt% PbO excess wet mixed with PSN powder (batch B) and isostatically pressed (Test7).

Figure 4.1.17 SEM image of cross section of PSN pellet sintered at 1250°C for 1 hour with a 4wt% planetary milled (30min) PbO excess wet mixed with planetary milled (30min) PSN powder and isostatically pressed (Test6).

As mentioned, Test0 showed secondary peaks corresponding to pyrochlore phases, while when adding a 4wt% PbO excess (Test1) the parasitic pyrochlore phase ($Pb_2Nb_2O_7$) could be eliminated. Figure 4.1.18 below shows the XRD patterns of Test0 and Test1. In addition to the impurities, Test0 also had a visible color gradient being darker in the center compared to the sides.
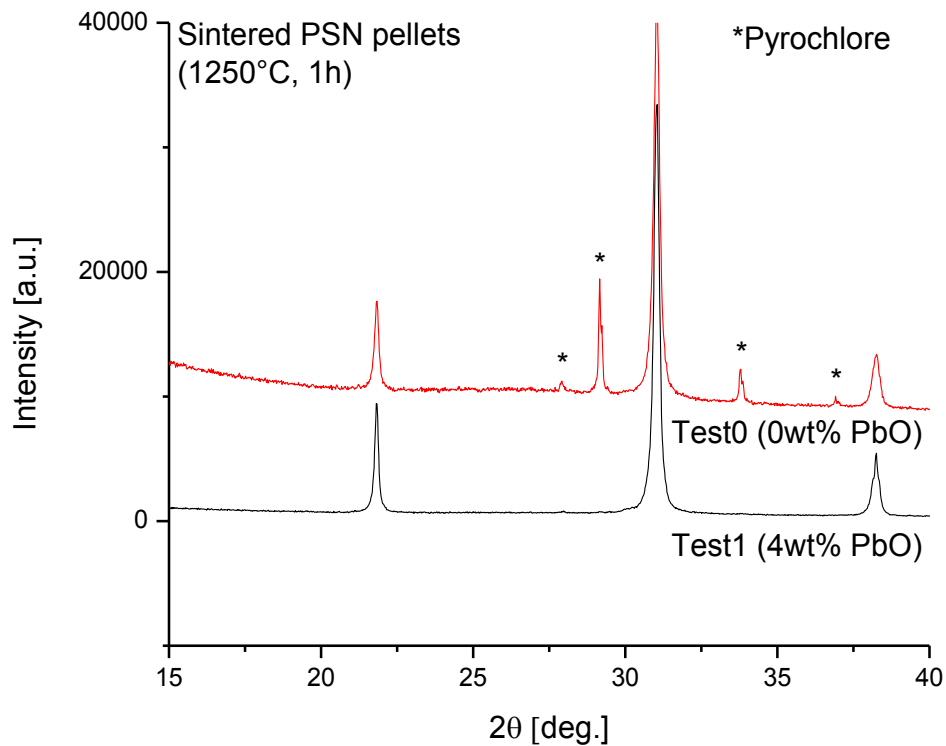
Figure 4.1.18 XRD patterns of Test0 and Test1 made with 0wt% and 4wt% PbO excess respectively. Both test samples were sintered for 1 hour at 1250°C.

Sintered PSN samples

Figure 4.1.19 shows the XRD patterns of sintered PSN (Sample1-3) pellets. All samples showed high purity with no secondary phases. No cation ordering could be observed after the sintering step. All peaks corresponded to the cubic Pm-3m (S.G. 221) of PSN. As shown in Table 4.1.3 the lattice constants were also within literature values.
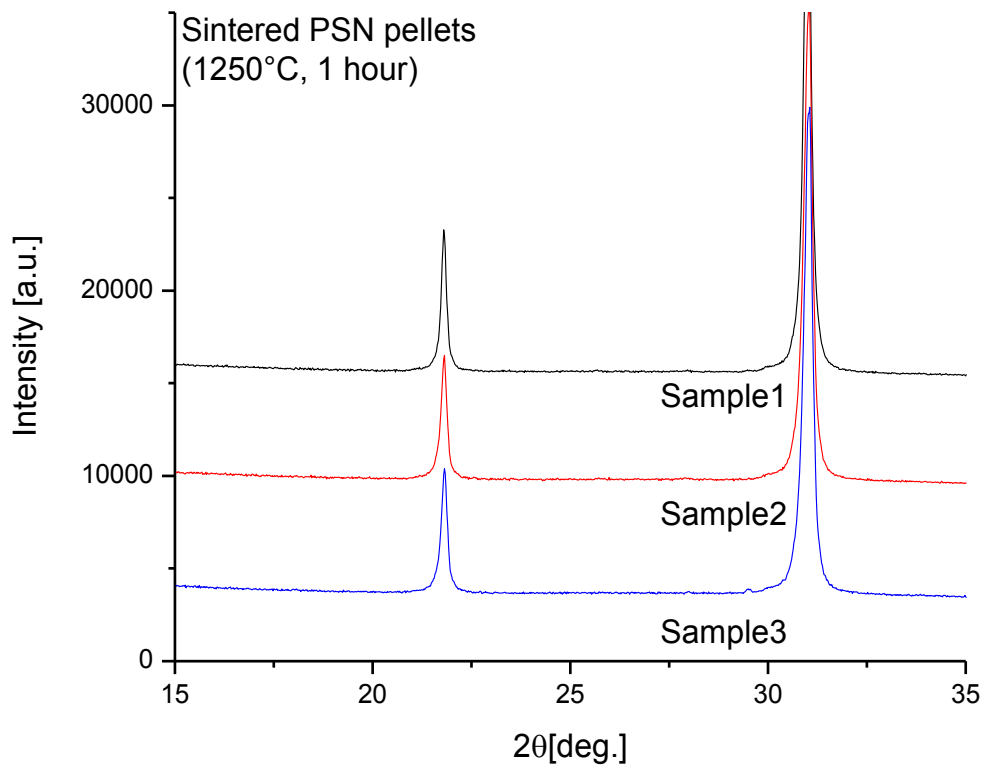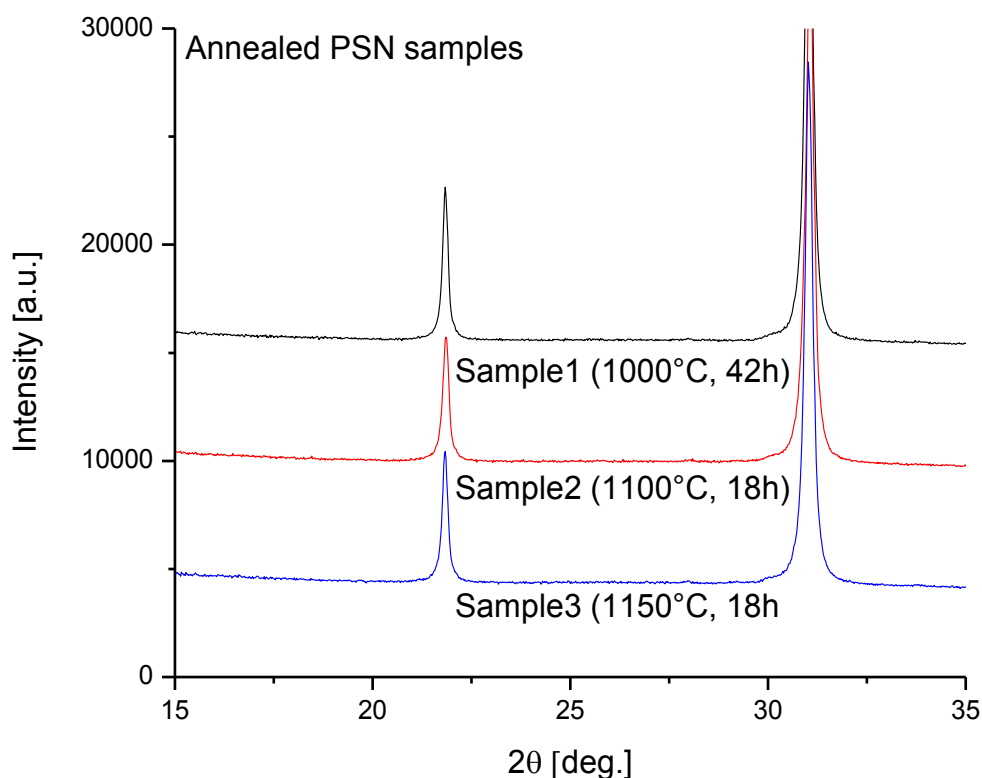

Figure 4.1.19 XRD patterns of PSN pellets sintered at 1250°C for 1 hour.

Annealing of PSN samples

Figure 4.1.20 shows the XRD patterns of Sample1 to Sample3 after annealing all samples at different temperatures and times. None of the samples showed any additional peaks corresponding to cation ordering. Sample2 and Sample3 also needed polishing on the sides. Pieces cracked off the sides during polishing, but as shown in Table 4.1.3, the density of the pellets were still high. Sample2 which was additionally annealed for 100 hours at 1100°C was bright yellow in color and contained large amounts of pyrochlore. A picture of the annealed samples is shown in Figure 4.1.21. Except from Sample2 which had changed color completely, Sample1 and sample3 had similar color. However, Sample1 was darker in the middle compared to the sides.

Figure 4.1.20 XRD patterns of PSN pellets after annealing for 42 hours at 1000°C (Sample1), 18 hours at 1100°C (Sample2) and 18 hours (Sample3) at 1150°C.

Figure 4.1.21 *Photograph of annealed PSN pellets (Sample1-3). The samples were annealed for 42h at 1000°C (Sample1, left), 18h + 100h at 1100°C (Sample2, middle) and 18h at 1150°C (Sample3, right).*

Lattice constants and densities of sintered and annealed samples

An increasing lattice constant was observed for almost all samples after annealing. The densities of Sample2 and Sample3 had increased almost 1% while Sample1 showed a reduction in density of more than 2%. The measured lattice constants were close to literature values ranging from 4.083Å to 4.087Å as shown in Table 4.1.3 below. There seemed to be a correlation between exposure to high temperature and lattice constant. Figure 4.1.22 shows that there was an observable increase in lattice constant throughout the processing steps, i.e., calcination, sintering and annealing, with Sample1 ending up with the largest lattice constant.

Table 4.1.3 *Densities and lattice constants of PSN pellets before and after annealing for a given temperature and time (T/t)*

| Property	Sample1	Sample2	Sample3
$\rho_{sintered}$	94.5%	92.7%	92.5%
T/t	1000°C/42h	1100°C/18h	1150°C/18h
$\rho_{annealed}$	92.3%	93.4%	93.2%
$a_{sintered}$[1]	4.087Å	4.083Å	4.084Å
$a_{annealed}$	4.087Å	4.085Å	4.086Å

1. Literature values of disordered PSN (S.G. 221, Pm-3m): (4.074Å [39] - 4.086Å [40]).
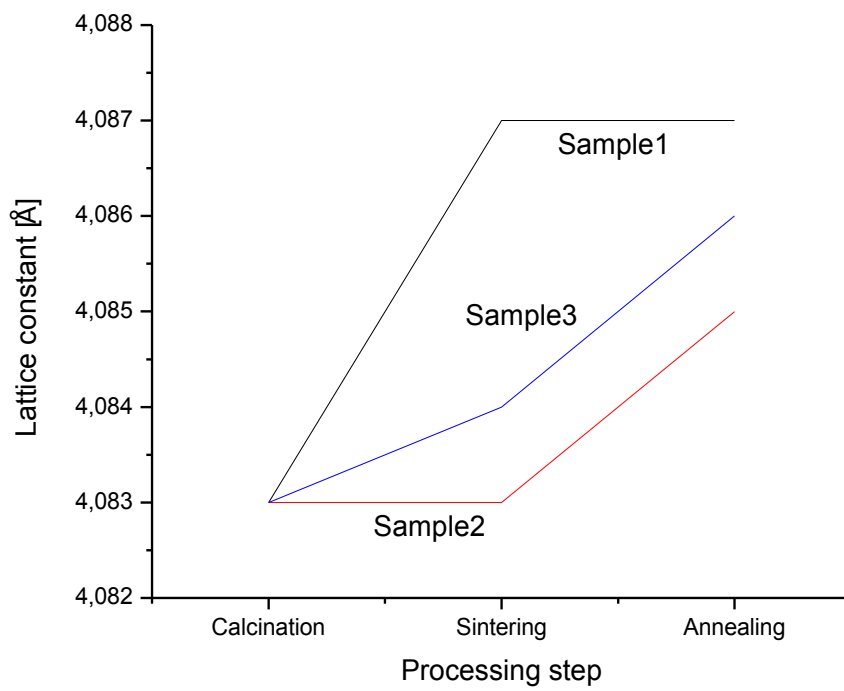
Figure 4.1.22 *Lattice constant as a function of processing step for Sample1, Sample2 and Sample3.*

Dielectric measurements

Figures 4.1.23- 4.1.26 shows the dielectric constant as a function of frequency and temperature. After annealing Sample1 there was an observable lowering in both the dielectric permittivity (ε') and the permittivity maxima temperature (T_m). A frequency dependence could be observed in all samples, also after annealing.
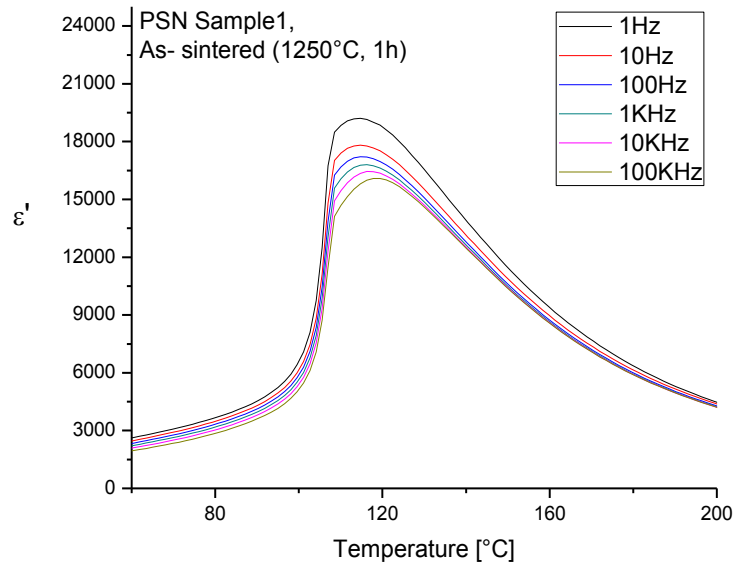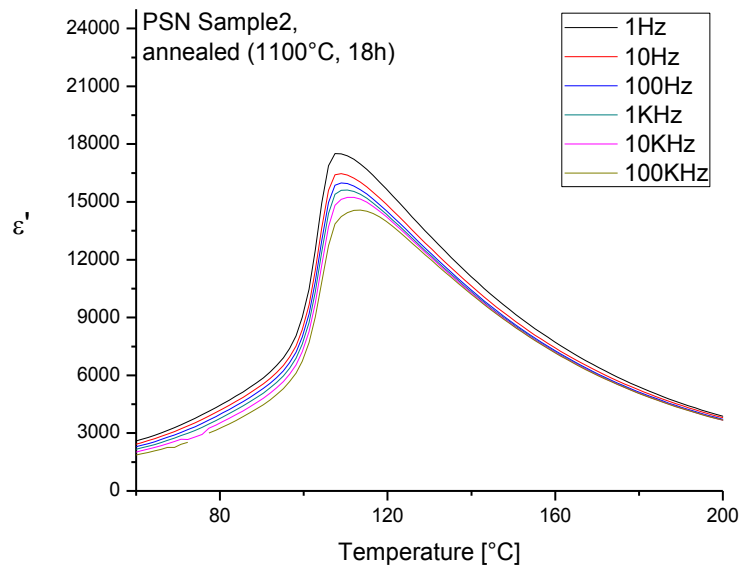

Figure 4.1.23 Dielectric measurements on as-sintered PSN pellet (Sample1)
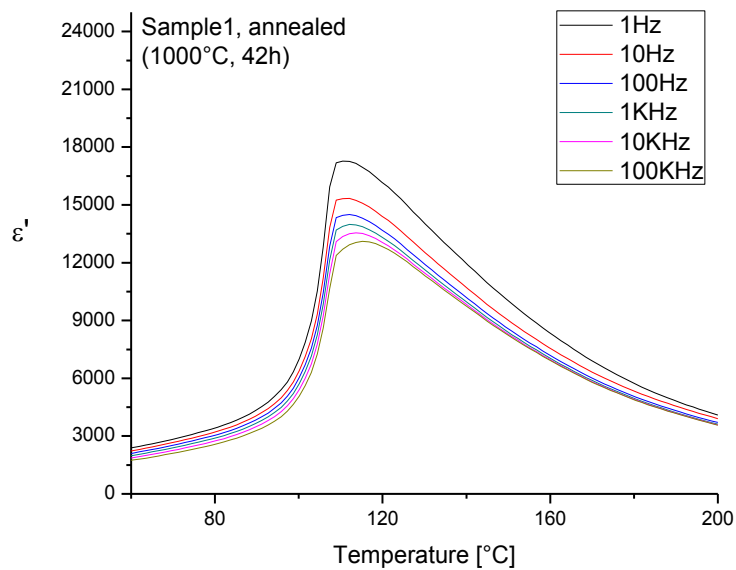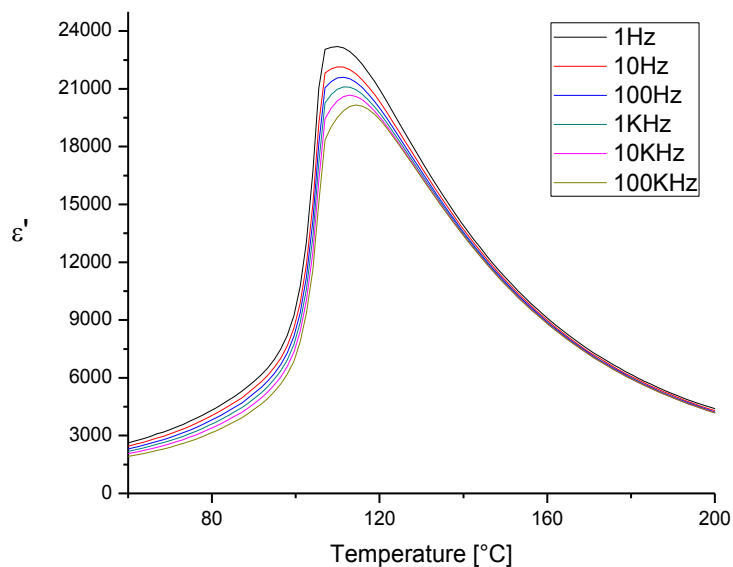

Figure 4.1.24 Dielectric measurements on PSN pellet annealed for 42 hours at 1000°C (Sample1).

Figure 4.1.25 and 4.1.26 shows the dielectric dispersion of Sample2 annealed for 18 hours at 1100°C and Sample3 annealed for 18 hours at 1150°C respectively. The permittivity maxima temperature T_m was lower compared to the as- sintered Sample1. However, Sample3 showed a significantly larger dielectric permittivity maxima (ε'_m) than all other samples.

Figure 4.1.25 Dielectric measurements on PSN pellet annealed for 18 hours at 1100°C (Sample2)

Figure 4.1.26 Dielectric measurements on PSN pellet annealed for 18 hours at 1150°C (Sample3).

Dielectric measurement values

The dielectric measurements revealed significant variations in both the permittivity maxima temperature and the permittivity maxima. Table 4.1.4 lists some important numbers retrieved from the dielectric measurements. Sample1 showed a lowering of both T_m and ε'_m. However, the frequency dependence ΔT_m had increased, which indicated a stronger relaxor behavior. Sample2 also showed a decrease in both values and an increasing frequency dependence when compared to the as- sintered Sample1. Sample3 showed a decrease in permittivity maxima temperature and an increase in the permittivity maxima. The frequency dependence of Sample3 was lower than that of Sample2, but still larger than the as- sintered Sample1. In general, annealing the samples resulted in a stronger relaxor behavior which was opposite to the expected. In addition, Sample3, which was also the thickest sample showed a significantly larger dielectric permittivity compared to the other annealed samples.

Table 4.1.4 *Different values extracted from the dielectric measurements*

Sample	Annealing	ε_m' (100KHz)	T_m (100KHz)	ΔT_m[1]
Sample1	X	16091.7	117.4	2.70
Sample1	1000°C, 42h	13107.2	114.8	4.29
Sample2	1100°C, 18h	14581.0	113.2	5.75
Sample3	1150°C, 18h	20164.0	114.0	4.06

1. Difference in T_m value at 100KHz and 1Hz.

4.2 Molten salt synthesis of PSN (Route 1)

Precursor phase purity

Figure 4.2.1 shows the diffraction patterns of the $ScNbO_4$ that was used in the molten salt synthesis of PSN. Also this batch needed several grounding and heating steps for the reaction to be complete, but after 7 grounding and heating steps, a phase pure precursor was obtained. The secondary phases observed were Nb_2O_5 and a non- stoichiometric scandium niobium oxide compound, $Sc_{5.5}Nb_{1.5}O_{12}$.
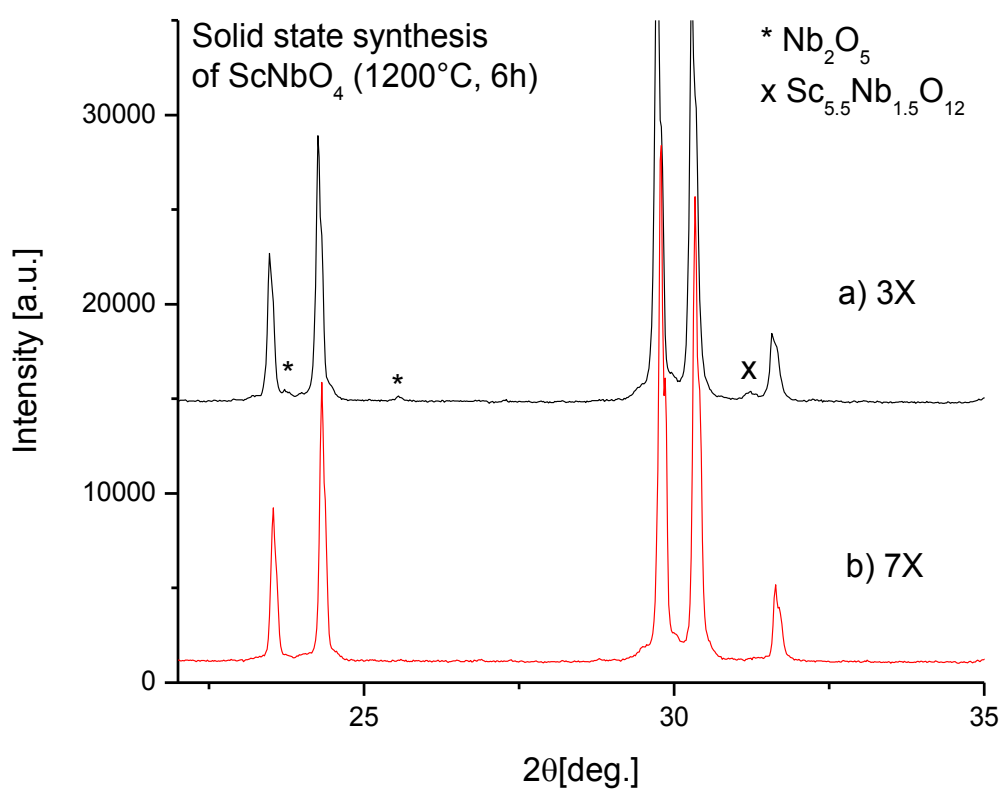
Figure 4.2.1 XRD pattern of $ScNbO_4$ precursor made at 1200°C for 6 hours after 3 (a) and 7 (b) times grounding and heating. Secondary phases are indicated with symbols.

PSN phase purity (Route 1)

Figure 4.2.2 below shows the diffraction patterns of the various PSN powders prepared at different temperatures, times and with varying heating and cooling rates. Neither the times, cooling- , or heating rates appeared to have an effect on the cation ordering as no superreflections were observed. However at 800°C and 1000°C secondary phases could be observed. The rest of the syntheses could be considered phase pure with a small amount of pyrochlore phases. At 800°C the secondary diffraction peaks corresponded to the $ScNbO_4$ precursor and PbO indicating that the reaction did not complete. One of the $ScNbO_4$ peaks coincided with a PbO diffraction peak. At 1000°C, the same diffraction peak appeared at the same angle. The peak was so small and the lack of other $ScNbO_4$ peaks made it difficult determine the phase with complete certainty.
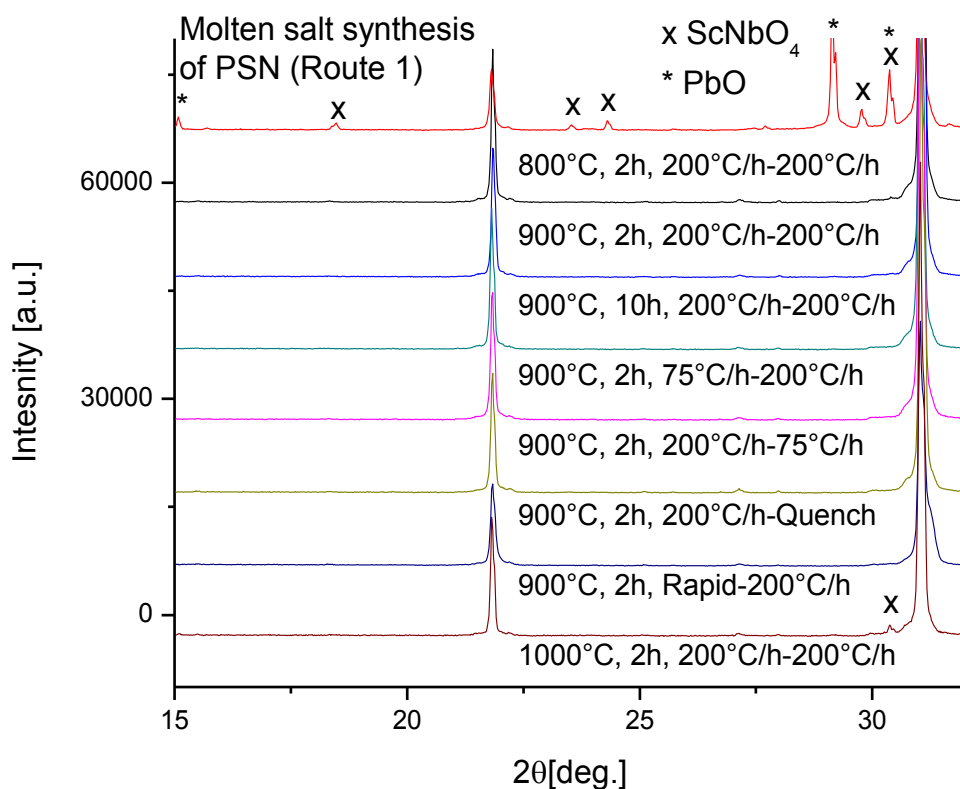
Figure 4.2.2 XRD patterns of molten salt synthesized PSN (Route 1) at different temperatures, times and heating/cooling rates. The parameters used are written under each diffraction pattern (heating temperature, hold time and heating-cooling rate. Secondary phases are indicated with symbols.

Figure 4.2.3 shows the diffraction patterns of the same syntheses as Figure 4.2.2 from 2θ=17°-22.5° with a logarithmic scale on the y-axis. Figure 4.2.3 shows that no diffraction peaks corresponding to superreflections could be observed. The secondary $ScNbO_4$ peak indicated in Figure 4.2.3 is from PSN synthesized at 800°C which can also be seen in Figure 4.2.2.
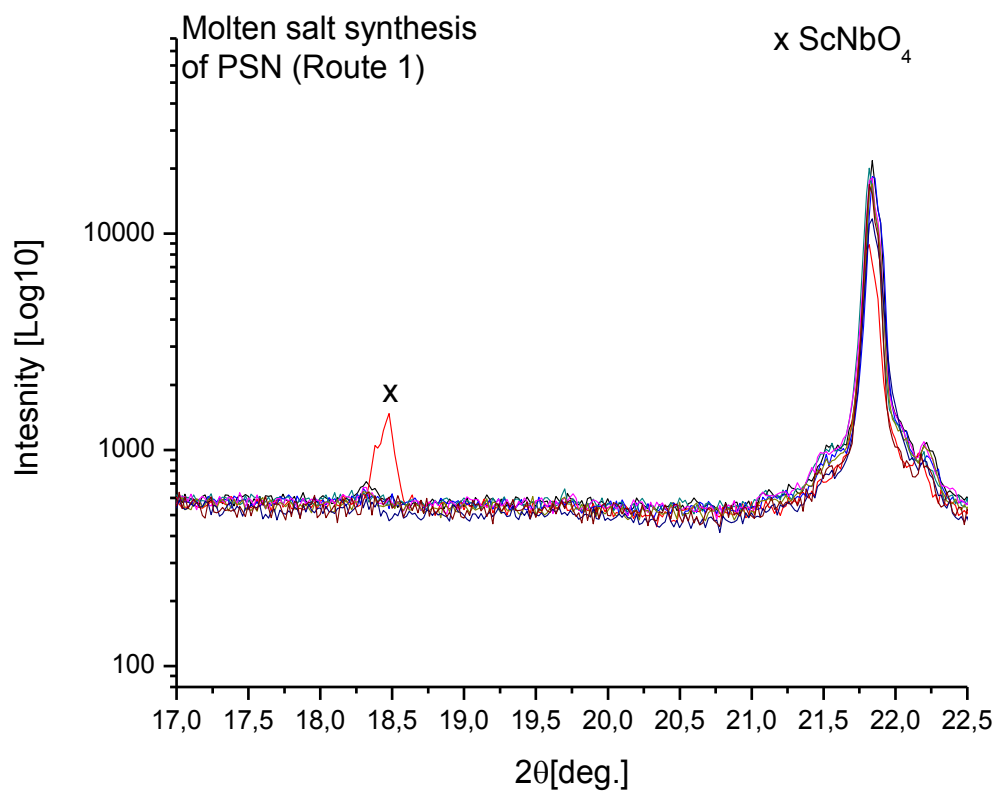
Figure 4.2.3 XRD patterns of molten salt synthesized PSN at different times, temperatures and heating- /cooling rates in the interval where B- cation ordering would be observed.

PSN particle size (Route 1)

SEM images of the molten salt synthesized PSN powder are shown in Figures 4.2.4- 4.2.9. From the images below it can be seen that there is a particle size increase when increasing the hold time from 2 hours to 10 hours. When comparing Figure 4.2.6 and 4.2.7 it looks like the air- quenching results in slightly larger particles. However, the heating rate shows a significant effect on the final particle size. Slow and fast heating results in large and small particle sizes respectively.
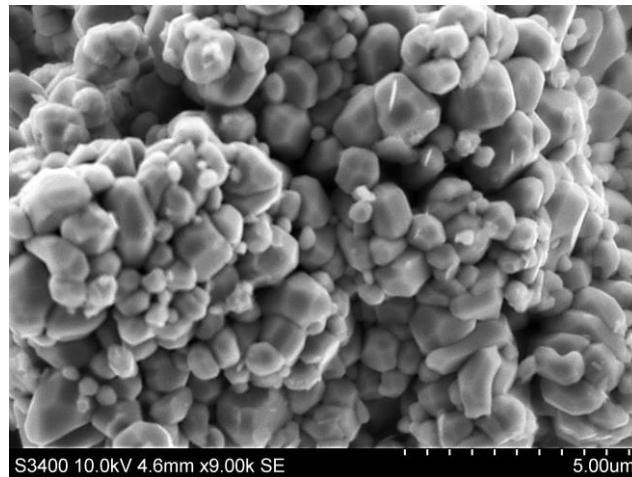
Figure 4.2.4 SEM image of molten salt synthesized PSN powder made at 900°C for 2 hours with a heating and cooling rate of 200°C/h. The salt to oxide weight ratio was 2:1.
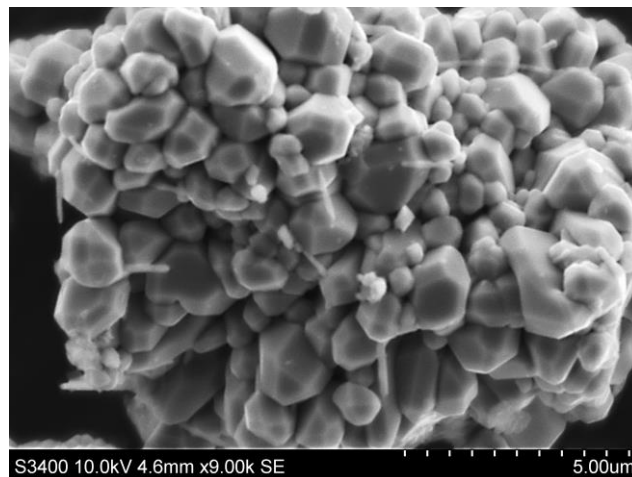
Figure 4.2.5 SEM image of molten salt synthesized PSN powder made at 900°C for 10 hours with a heating and cooling rate of 200°C/h. The salt to oxide weight ratio was 2:1.
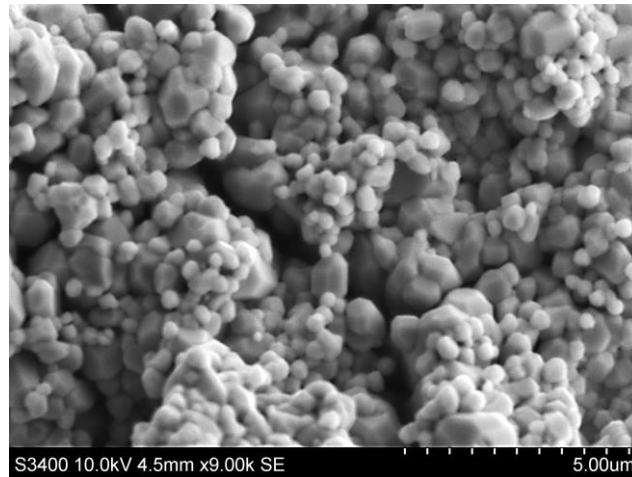
Figure 4.2.6 SEM image of molten salt synthesized
PSN powder made at 900°C for 2 hours with a
heating and cooling rate of 200°C/h and 75°C/h
respectively. The salt to oxide weight ratio was 2:1.

Figure 4.2.7 SEM image of molten salt synthesized
PSN powder made at 900°C for 2 hours with a
heating rate of 200°C/h and open air cooling. The salt
to oxide weight ratio was 2:1.
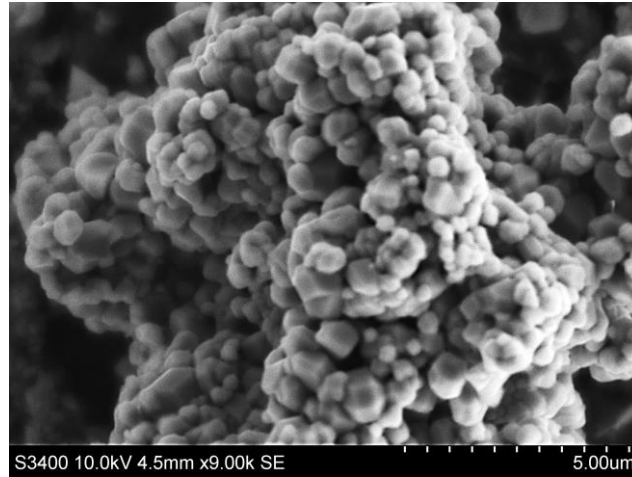
Figure 4.2.8 SEM image of molten salt synthesized PSN powder made at 900°C for 2 hours. The crucible was put into a preheated oven holding 900°C and cooled at a rate of 200°C/h. The salt to oxide weight ratio was 2:1.
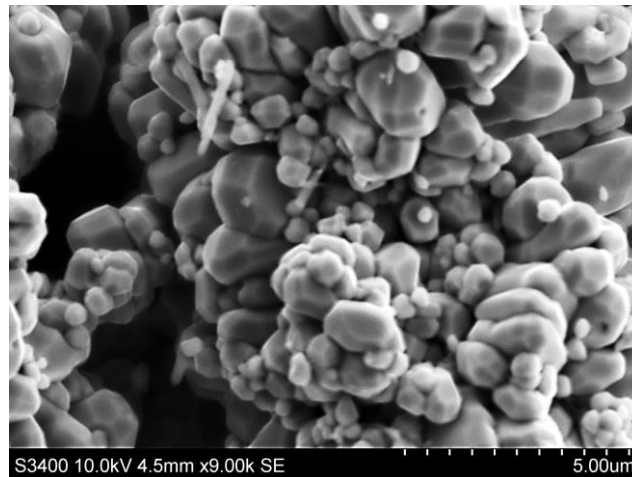
Figure 4.2.9 SEM image of molten salt synthesized PSN powder made at 900°C for 2 hours with a heating and cooling rate of 75°C/h and 200°C/h respectively. The salt to oxide weight ratio was 2:1.

Figure 4.2.10 shows the PSN particle sizes when prepared at 800°C. There were smaller particles growing on top of bigger particles, and the bigger particles were comparable in size with the ScNbO$_4$ precursor shown in Figure 4.1.2. At 1000°C the particles were large and the particle size distribution had narrowed significantly.
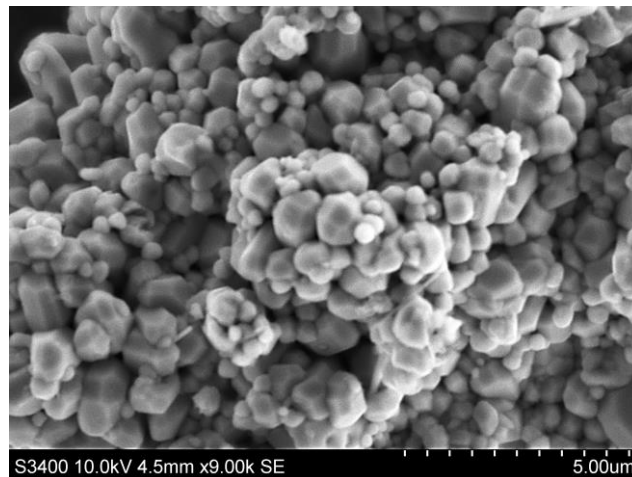

Figure 4.2.10 SEM image of molten salt synthesized PSN powder made at 800°C for 2 hours with a heating and cooling rate of 200°C/h. The salt to oxide weight ratio was 2:1.

Figure 4.2.11 SEM image of molten salt synthesized PSN powder made at 1000°C for 2 hours with a heating and cooling rate of 200°C/h. The salt to oxide weight ratio was 2:1.

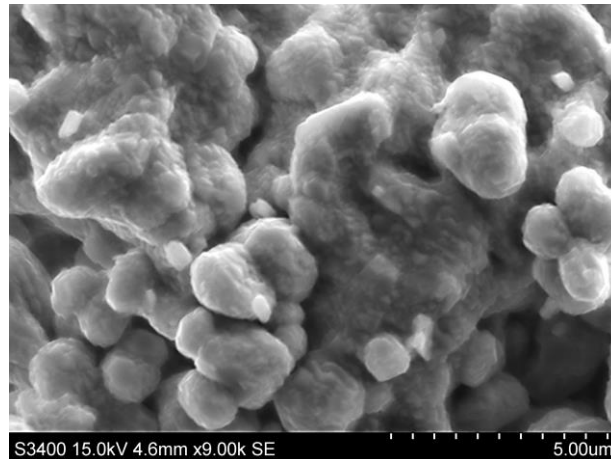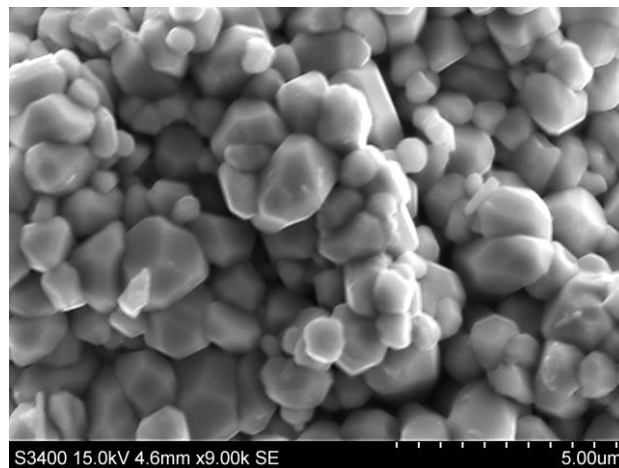**PSN lattice constant and crystallite size (Route 1)**

Table 4.2.1 below shows the average crystallite sizes and lattice parameters from Rietveld refinement. The time, temperature and heating rate effect on particle sizes can to some extent be found in the calculated average crystallite sizes. When increasing the time from 2 hours to 10 hours, the crystallite size increases. Also when the temperature is increased from 900°C to 1000°C, the crystallite size increases. When looking at the heating rates, it can be seen that a faster heating rate (Rapid) gives smaller crystallite size than when slow heating (75°C/h). The lattice constants varied but were within literature values of disordered PSN. Ranging from 4.077Å to 4.082Å most were in the lower range of the reported lattice constants of both ordered and disordered PSN. The most important observation was that the smallest lattice constant was observed for the synthesis with the smallest calculated crystallite size, in this case for (900°C 2h, 2-1 200°C/h-200°C/h). The lattice constants were plotted against crystallite sizes and are shown in Figure 4.2.12. With this few values it was difficult to see a significant relationship as the uncertainty was too large. However, the smallest and largest lattice constants were measured for small and large crystallite sizes respectively.

Table 4.2.1 PSN average crystallite sizes and lattice constants from Rietveld refinement of PSN powder synthesized through route 1 with varying heating- and cooling rates, times and temperatures.

Synthesis	Crystallite size (nm)	a (Å)[1]
800°C 2h, 2-1, 200°C/h-200°C/h	157[2]	4.082[2]
900°C 2h, 2-1 200°C/h-200°C/h	112	4.077
900°C 10h, 2-1 200°C/h-200°C/h	262	4.080
900°C 2h, 2-1 75°C/h-200°C/h	230	4.081
900°C 2h, 2-1 Rapid-200°C/h	138	4.078
900°C 2h, 2-1 200°C/h-75°C/h	202	4.081
900°C 2h, 2-1 200°C/h-Quench	220	4.078
1000°C 2h, 2-1 200°C/h-200°C/h	311	4.080

1. Literature values of disordered PSN (S.G. 221, Pm-3m): (4.074Å [39] - 4.086Å [40]). 2. Synthesis was not phase pure.
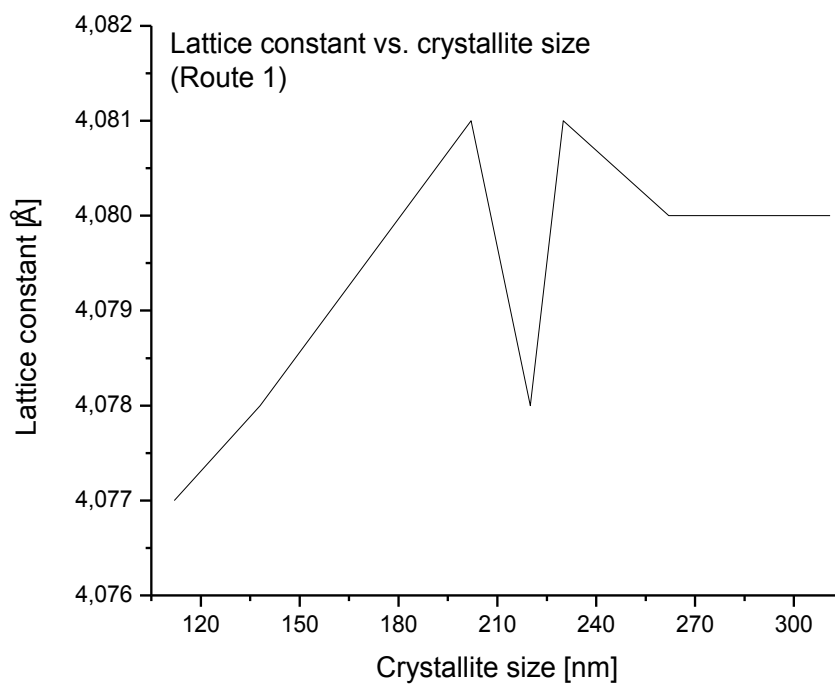
Figure 4.2.12 *Lattice constant as a function of crystallite size (Route 1)*

54

4.3 Molten salt synthesis of PSN (Route 2)

PSN phase purity (Route 2)

Figure 4.3.1 below shows the XRD patterns from the molten salt synthesis of PSN without using the ScNbO$_4$ precurcor. When comparing with the XRD patterns from Figure 4.2.2, smaller amounts of at least one unknown secondary phase was observed when using route 2, and no cation ordering could be observed. The secondary peaks coincided with both ScNbO$_4$ and PbO peaks. However, the lack of the PbO and ScNbO$_4$ peak at 2θ≈29° seen in Figure 4.2.2 in Route 1 made it difficult to confirm the phase. Also, two of the syntheses did not show the secondary peaks and they did not seem to be correlated to any of the varied parameters.
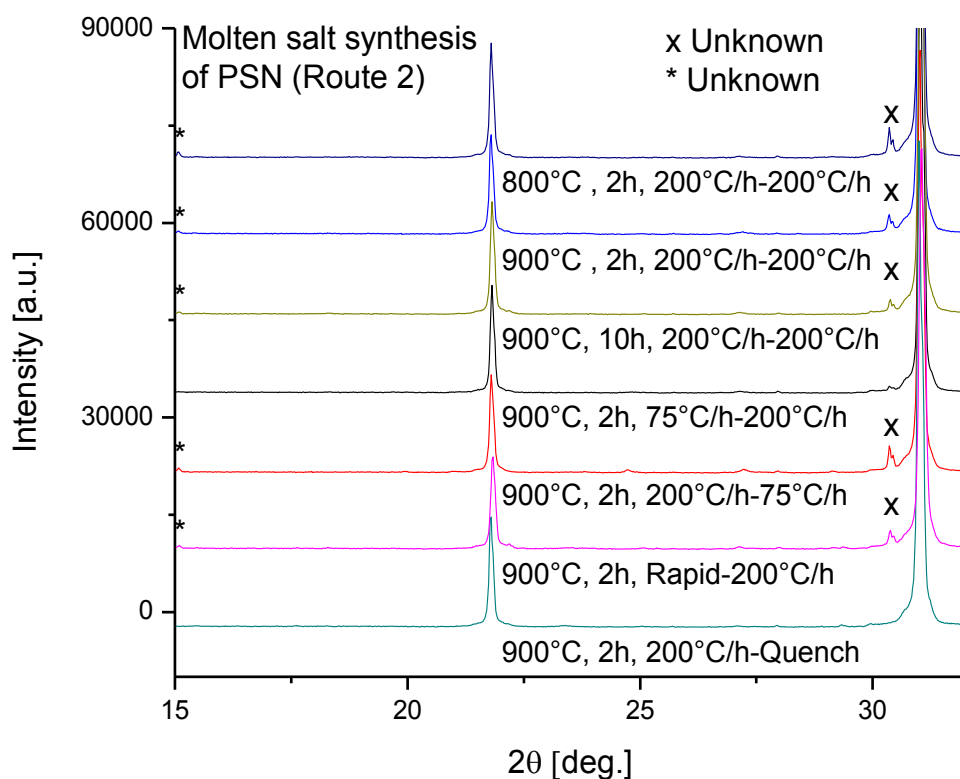
Figure 4.3.1 XRD patterns of molten salt synthesized PSN (Route 2) at different temperatures, times and heating/cooling rates. The parameters used are written under each diffraction pattern (heating temperature, hold time and heating-cooling rate. Secondary phases are indicated with symbols.

Figure 4.3.2 shows the diffraction patterns of the same syntheses as Figure 4.3.1 from 2θ=17°-22.5° with a logarithmic scale on the y-axis. Similar for both Route 1 and Route 2 was that no cation ordering was observed.
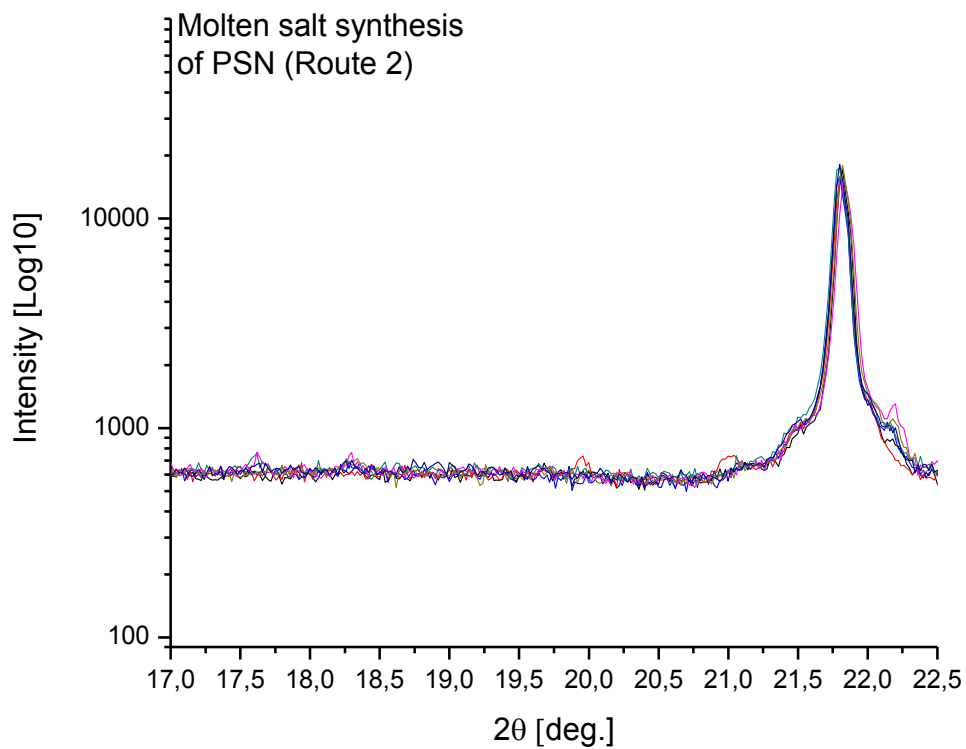
Figure 4.3.2 *XRD patterns of molten salt synthesized PSN (Route 2) at different times, temperatures and heating- /cooling rates in the interval where B- cation ordering would be observed.*

PSN particle size (Route 2)

From Figure 4.3.3 to 4.3.8 it can be seen that when using Route 2 the particle sizes are consequently smaller than when using the *Wolframite method* with the ScNbO$_4$ precursor (Route 1). As expected, the particle size increased with heating time. Furthermore, only when comparing Figure 4.3.7 and 4.3.8, with fast and slow heating rate respectively, a significant size difference can be observed. Slower and faster heating rates also here resulted in larger and smaller particles respectively. The same tendency was observed for the crystallite sizes listed in Table 4.3.1.
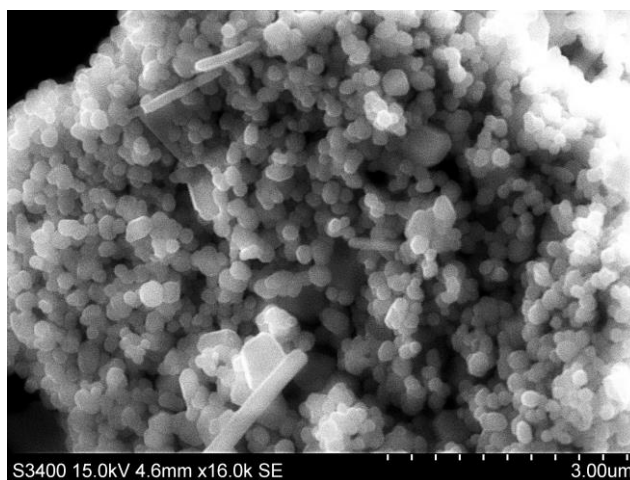
Figure 4.3.3 SEM image of molten salt synthesized PSN powder made at 900°C for 2 hours with a heating and cooling rate of 200°C/h. The salt to oxide weight ratio was 2:1.
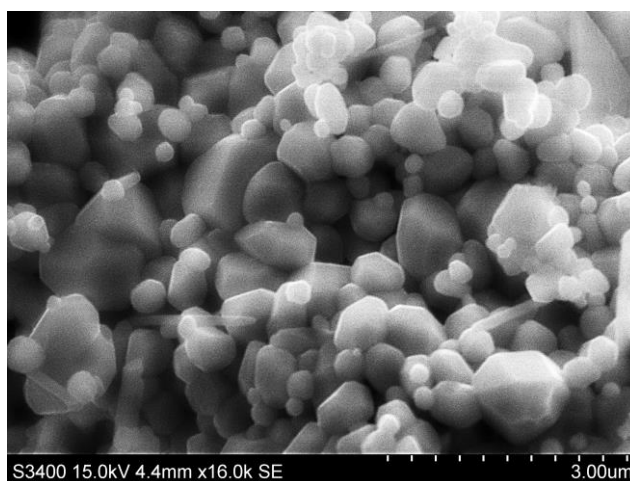
Figure 4.3.4 SEM image of molten salt synthesized PSN powder made at 900°C for 10 hours with a heating and cooling rate of 200°C/h. The salt to oxide weight ratio was 2:1.
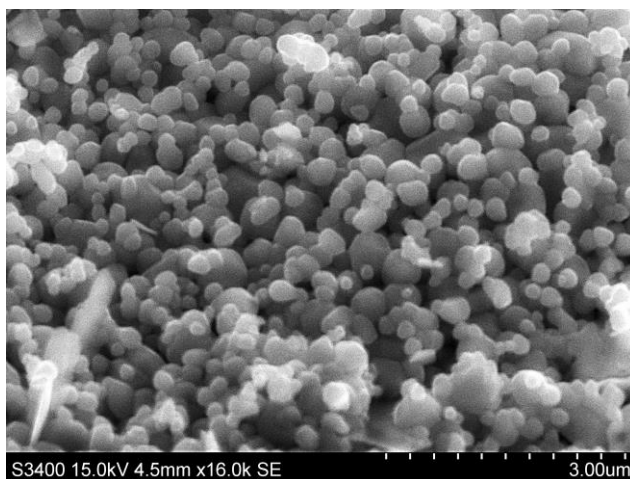
Figure 4.3.5 SEM image of molten salt synthesized PSN powder made at 900°C for 2 hours with a heating and cooling rate of 200°C/h and 75°C/h respectively. The salt to oxide weight ratio was 2:1.
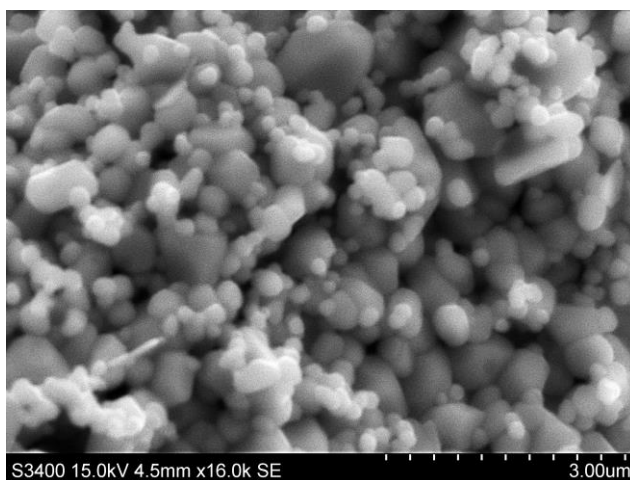
Figure 4.3.6 SEM image of molten salt synthesized PSN powder made at 900°C for 2 hours with a heating rate of 200°C/h and open air cooling. The salt to oxide weight ratio was 2:1.
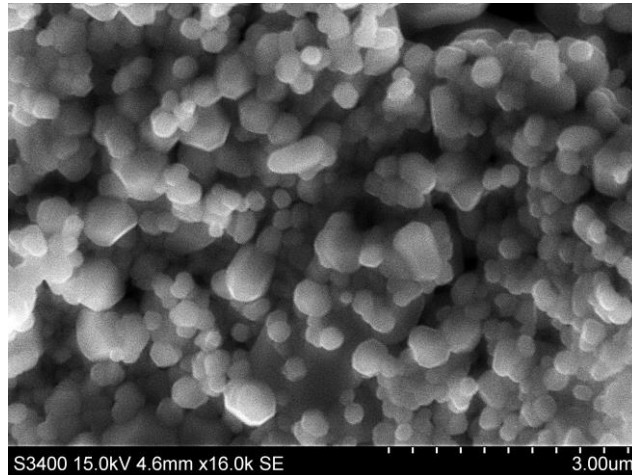
Figure 4.3.7 SEM image of molten salt synthesized
PSN powder made at 900°C for 2 hours. The crucible
was put into a preheated oven holding 900°C and
cooled at a rate of 200°C/h. The salt to oxide weight
ratio was 2:1.
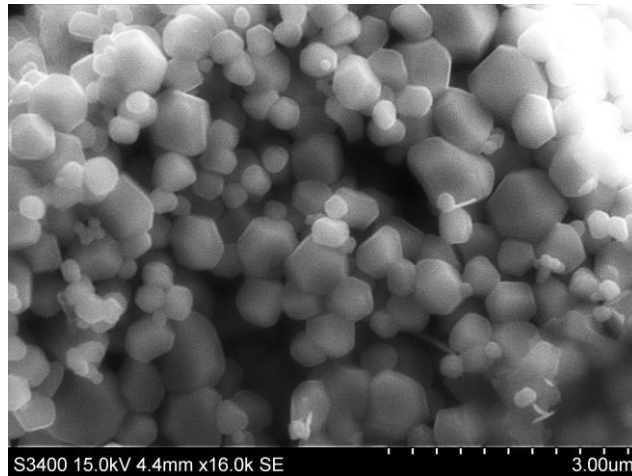
Figure 4.3.8 SEM image of molten salt synthesized
PSN powder made at 900°C for 2 hours with a
heating and cooling rate of 75°C/h and 200°C/h
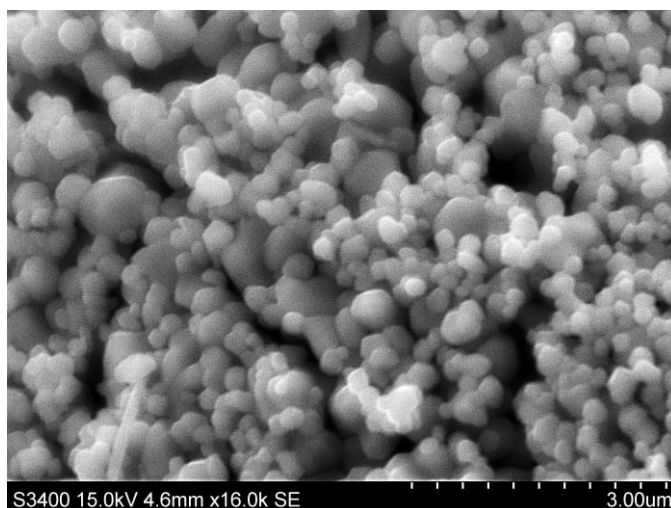
Figure 4.3.9 *SEM image of molten salt synthesized PSN powder made at 800°C for 2 hours with a heating and cooling rate of 200°C/h*

PSN lattice constants and crystallite sizes (Route 2)

From Table 4.3.1 below, the effect of heating and cooling rates, time and temperature on crystallite size and lattice parameter can be seen. While heating rates at 200°C/h resulted in similar crystallite sizes, independent of cooling rate and total synthesis time, fast and slow heating rates, resulted in smaller and bigger particle and crystallite sizes respectively. The lattice constants retrieved from Rietveld refinement had less variations compared to route 1. They were all smaller than the literature value of disordered PSN and closer to the ordered PSN from the last study which measured 4.076Å [7]. The smallest lattice constant was also here observed for the PSN powder with the smallest calculated crystallite size, in this case for (900°C 2h, 2-1 Rapid-200°C). However, Figure 4.3.10 shows that no significant trend could be observed when comparing lattice constants and crystallite sizes, but also here small and large lattice constants were measured for small and large crystallite sizes.

Table 4.3.1 *PSN crystallite size and lattice parameters from Rietveld refinement of PSN powder synthesized through route 2, with varying heating- and cooling rates, times and temperatures.*

Synthesis	Crystallite size (nm)	a (Å)[1]
800°C 2h, 2-1, 200°C-200°C	169	4.079
900°C 2h, 2-1 200°C-200°C	164	4.080
900°C 10h, 2-1 200°C-200°C	162	4.080
900°C 2h, 2-1 75°C-200°C	198	4.079
900°C 2h, 2-1 Rapid-200°C	144	4.078
900°C 2h, 2-1 200°C-75°C	164	4.079
900°C 2h, 2-1 200°C-Quench	165	4.080

1. Literature values of disordered PSN (S.G. 221, Pm-3m): (4.074Å [39] - 4.086Å [40]). 2. Synthesis was not phase pure.
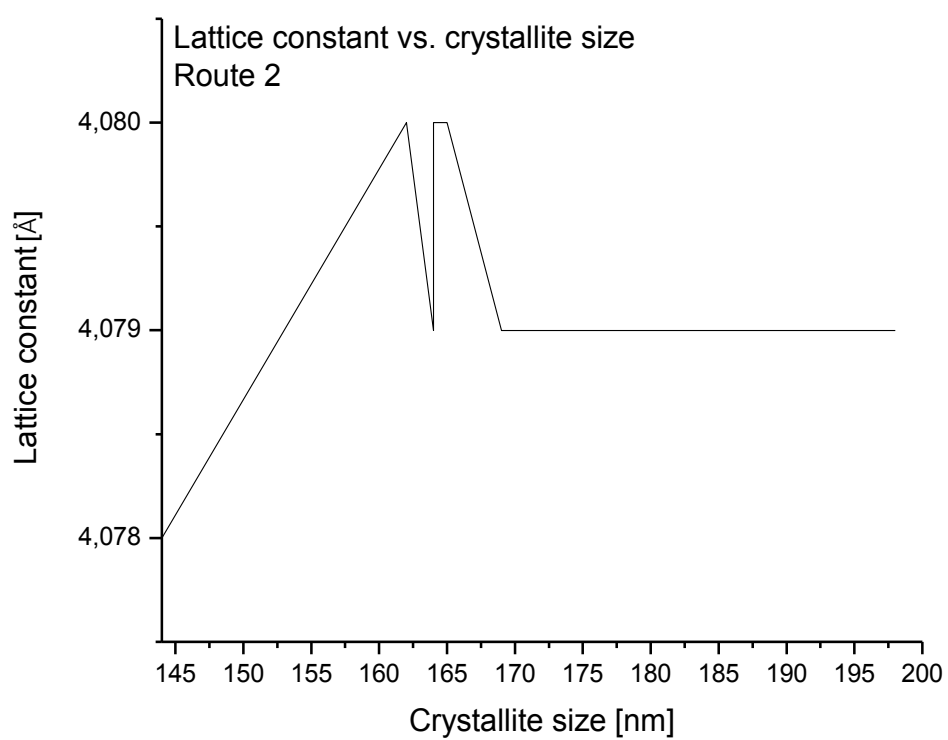
Figure 4.3.10 *Lattice constant as a function of crystallite size (Route 2)*

5. Discussion

By using the conventional mixed oxides method (Route 2) and the *Wolframite method* (Route 1), phase pure PSN was successfully synthesized by molten salt synthesis using 0.50NaCl-0.50KCl salt combination. Neither methods showed any signs of cation ordering, though time, temperature and heating rate had an effect on particle and crystallite sizes, and lattice constants. In both route 1 and 2, fast and slow heating rates resulted in small and large particles respectively. For route 2, the difference between heating- and cooling rate was independent of total heating time and the cooling rate. Route 1 however, showed a certain heating time dependence. The *Wolframite method* also consequently yielded larger particle and crystallite sizes in almost all cases. Both routes had PSN lattice constants that were within the limit of literature values. The smallest lattice constants were observed for the PSN powder with the smallest measured crystallite sizes, but no significant correlation between crystallite size and lattice constant could be measured.

Calcined phase pure PSN powder from solid state synthesis was pressed into pellets using different parameters and different amounts of excess PbO. After several attempts, three phase pure and dense PSN pellets could be made when using a 4wt% PbO excess. The three samples were then annealed at different temperatures and times to obtain cation ordering. After annealing Sample2 and Sample3 for 18 hours at both 1100°C and 1150°C, no cation ordering could be observed from the XRD patterns. However, the dielectric measurements showed a reduction in the permittivity maxima temperature T_m compared to the as- sintered Sample1. Sample3 however, showed a larger dielectric permittivity maxima than Sample2. The lowering of these values are related to cation ordering but may also be caused by lead vacancies. When annealing Sample1 at 1000°C for 42 hours, a reduction in both values was observed as well. However, common for all samples after annealing, was the increasing frequency dependence ΔT_m which suggests an increasing relaxor behaviour which is not seen in ordered PSN. In addition there was observed a clear correlation between the increasing PSN lattice constants and heat exposure during the processing steps.

5.1 Molten salt synthesis of PSN

Phase purity

There was an observable difference in purity between the two routes with route 1 giving the more pure PSN powder. However, at 800°C the reaction did not complete, leaving unreacted $ScNbO_4$ and PbO which could be detected as secondary peaks in the XRD. Here route 2, gave the more pure product of the two routes. However, almost all other syntheses following route2 showed secondary peaks coinciding with the $ScNbO_4$ and PbO peaks. These peaks could also be seen in route 1 at 1000°C, but there seemed to be no correlation between them. However, the fact that they appear at 1000°C in route 1, may be related lead evaporation resulting in non- stoichiometry and therefore other compounds with similar structure to the precursor and PbO.

The pure PSN obtained using route 2 appeared when quenching and slow heating the molten salt mixture. A possible explanation for this cannot be provided. Nevertheless, the incomplete reaction at 800°C (Route 1) may be used to explain some important synthesis details. The fact that route 2 apparently resulted in the largest amount of unused reactants, may be explained by the different reaction rates in the two routes. As will be discussed next, SEM images will provide useful information regarding the most probable limiting factor that eventually results in bigger PSN particles for route 1.

Particle size and reaction rates

At all times, temperatures and heating and cooling rates, the particle sizes were consequently larger when the $ScNbO_4$ precursor was used. SEM images of PSN synthesized at 800°C can be used to explain this feature. The images revealed smaller particles growing on top of bigger particles which were comparable in size with the $ScNbO_4$ precursor. It is therefore highly probable that these precursor particles act as nucleation sites and that the PSN particles nucleate and grow on these particles. From the fact that the precursor particles were repeatedly synthesized at high temperatures for 6 hours, it is reasonable to assume that they were much larger than the constituting reactants Sc_2O_3 and Nb_2O_5. From the theory section on molten salt synthesis, we know that the PSN particles are likely to nucleate heterogeneously on the least soluble reactant. Evidently, the precursor is the least soluble of the reactants and therefore work as nucleation sites for PSN. Even more exciting information can be drawn from these facts. The size of the nucleation sites is here bound to determine the reaction rates. Therefore, from the argumentation above, the lower reaction rate when using route2 comes as no shock, but rather reflects the importance of reacting powder particle size. From the SEM images of PSN synthesized at 800°C this is made visible as the smaller surface area of the large precursor particles are covered with nucleating PSN particles. This leaves a large amount of precursor unexposed to PbO particles to form PSN. Summarized shortly; the larger the nucleation sites, the lower the reaction rates. When

recognizing that there are inevitably fewer nucleation sites when using route1, the reason for the consequently larger particles can also be understood.

Lattice constants and crystallite size

When looking at the lattice constants obtained from experimental results, they were all in the lower range of reported values and also lower than those of solid state synthesized PSN, which at least is a step in the right direction.

The lattice constants were very similar, and there was only one parameter that stuck out as a common factor for the two routes. The smallest lattice constant was obtained for the PSN powder that had the smallest calculated crystallite sizes. However, plotting the lattice constants as a function of crystallite sizes did not reveal a significant correlation. A possible explanation for the smaller lattice constant was also difficult to relate to the synthesis parameters. It should though be pointed out that both routes yielded larger and smaller crystallite sizes for fast and slow heating rates. However, it may have been due to the difference in total heating time, which is a well-known parameter that increases particle size. But the measured crystallite sizes in route 2, seemed independent of cooling rates and total heating time. In route 1 however, the total heating time did make a difference, which as explained above was likely to be caused by the larger precursor particles slowing down the reaction rates. Whether heating rate can be used to influence cation ordering is still unclear and will be shed light on next.

Cation ordering

No cation ordering could be observed in the molten salt synthesized PSN. As mentioned in our earlier study [7], the lack of ordering is likely to be controlled by the kinetics. From a thermodynamic consideration, the synthesis temperature is well below the order- disorder temperature, which should lower the entropy contribution to Gibbs free energy.

Both with and without the precursor, PSN formation is a fairly fast process while ordering by annealing is a very slow process. However, during our earlier study we were able to detect a small secondary peak corresponding to the PSN superstructure. Due to a mistake, this synthesis was conducted with a slightly different salt combination, 0.44NaCl-0.56KCl compared to 0.5NaCl-0.5KCl. All combinations of NaCl-KCl different from the eutectic 0.50-0.50 combination has a higher melting point. With this in mind, an explanation to the cation ordering in the earlier study, may be that the kinetics were slower and therefore the B-cations had longer time to find the most energetically favored site in the crystal lattice. As this was the only difference between the two syntheses, no other explanation can be given. For this reason, it is likely that a different order- disorder temperature exist in the molten salt

system. This order- disorder temperature should be dependent on both the salts and how they are combined.

5.2 Solid state synthesized PSN

Sintering

The variations in sintered pellet density was difficult to link to any of the varied parameters. SEM images of PSN powder batch B gave the impression of slightly lower degree of agglomeration, which is preferred when making high density materials. The temperature used to make batch B was 100°C higher than for batch A which should have given smaller particles for batch A, as temperature is usually the most important factor. However, the crystallite sizes obtained from Rietveld refinement were very similar, thus we may assume that the shorter time also kept the degree of agglomeration at an almost similar level. After milling PSN batch A however, the degree of hard agglomerates was reduced significantly, which according to theory should have given batch A an advantage. But milling did not seem to have an effect on the pellet density, although the open porosity was reduced slightly. Test0 measured the lowest density of all the test samples, while when introducing a PbO excess, the density went up in agreement with theory. Wet mixing the excess PbO with PSN was also effective in increasing the density as well as reducing the open porosity. This can be explained by a more homogeneous distribution of PbO and a homogeneous liquid phase sintering effect. However, SEM cross- section images did not show a significant difference in pore distribution and could therefore not confirm this.

As mentioned in the theory, the liquid PbO may increase the contact pressure between the PSN particles and thereby work as a sintering aid. For Test3 and Test4, in which PSN was wet mixed with the PbO excess, both measured higher densities, in agreement with theory and the assumption of a more homogeneous liquid phase sintering. Both test samples showed higher densities than the dry mixed Test0, Test1 and Test2. Also, Test4 which was made with PbO excess of 8wt%, showed the highest density of all pellets made with PSN batch A. This supports the assumption of PbO increasing the liquid phase sintering even more. However, the large amount of PbO excess resulted in large dense areas, but Test4 also measured the largest pore sizes. This may also explain why test4 showed an increase in open porosity compared to Test3 which was made with half the amount of excess PbO. The pore sizes of all test samples were comparable in size and shape with the PbO particles. For that reason, it may be that the PbO particles left irregularly shaped voids as the PbO melted. The SEM images of PbO did indeed look irregularly shaped, both before and after milling. From theory we know that these Irregular and flat pores are more difficult to remove during sintering and therefore more likely to stay as they were. However, Test5 which was made with milled PbO displayed a large increase in open porosity which was difficult to explain. Had Test5 showed a reduction in open porosity only, it would have been easier to relate to the more regular shaped PbO particles. But because of the large measured open porosity, Test5 was intentionally cracked with a hammer to investigate a smaller piece of the pellet to see if the low density was due to internal cracks or voids. The density of the smaller piece had similar density and a large open porosity. Therefore, internal cracks or voids were less likely to have

been the cause. If the pellet did have internal voids or cracks, they should have been exposed during cracking. However, Test6 which was made similar to Test5, with an additional cold isostatic pressing step, showed a reduction in open porosity. The large open porosity in Test5 may therefore be explained by some defects introduced to the pellet during pressing and that they were not exposed during cracking. While in Test6, these defects could be eliminated by the additional cold isostatic pressing step. Or at least they were locked inside to only yield closed porosity, as the closed porosity was larger in Test6. Therefore, although densities were measured as a function of load to find the ideal pressure, there were still an unknown parameter causing low density pellets.

PSN batch B however, was tested with a better result. The open porosities were low, the densities reached above 92% and the pellets did not crack. A good explanation for this can unfortunately not be given.

Although all the final samples used for dielectric measurements showed fairly high densities with low open porosity, Sample1 had a higher density than the two other samples after sintering. This may be related to the different thickness during sintering, where Sample1 was the thinnest of the samples. The difference in thickness was merely a result of the different amount of PSN powder used. The difference in densities may therefore have been a result of the sintering time or temperature being better suited for a thinner pellet. However, the densities measured after annealing Sample2 and Sample3 showed an increasing density, while Sample1 decreased after annealing. The most reasonable explanation for the difference after sintering, is therefore the thickness, and the higher surface to volume ratio of Sample1. The two other samples were thicker during sintering and had therefore a smaller surface to volume ratio. In the next sections, argumentation for this being related to a higher PbO evaporation will be presented, and as we will see, it may have affected other material properties as well. The low density areas in Test6 and the photograph of Sample1 after annealing may also support this.

The density of the calcined PSN pellets showed a very low density of only 40% of theoretical density. This also agrees well with the theory on PbO and its effect on sintering and swelling properties. The pellets showed an increased volume or swelling which may be explained by PbO evaporation which is discussed next.

PbO excess and purity

The calcined PSN pellet most likely swelled due to PbO evaporation as explained in the theory section. Still, the XRD data showed a phase pure PSN which should be kept in mind for the later discussion. Both calcined PSN batches A and B showed similar phase purity with no secondary phases detected in the XRD.

When the powder thereafter was used for sintering at higher temperatures, Test0 showed a secondary phase with a lower lead content. This secondary phase ($Pb_2Nb_2O_7$) also has a lower density than PSN, which supports the fact that Test0 also measured the lowest density. However, after mixing in a PbO excess (Test1), the PSN pellets could be considered phase pure. Even though the excess PbO conflicts with the stoichiometry, this study confirms the importance of a PbO excess during sintering of lead containing materials. The excess PbO is not only important for the density and liquid phase sintering, but also highlighted now, the phase purity. The excess PbO is effective in eliminating the pyrochlore phases which are known to reduce the dielectric permittivity. This study also shows that there is no residual PbO detected by the XRD. Due to the high sintering temperatures, PbO evaporates in the sealed alumina crucible which is bound to create a higher pressure of PbO inside. This way, the driving force for lead vacancies being introduced to the PSN crystal lattice during sintering should be reduced. It should also be remembered that the calcination step was conducted using two alumina crucibles, with a larger amount of PbO powder in the outer crucible, which should have created an even higher PbO vapour pressure outside the inner crucible.

Increasing lattice constants

The calcined PSN batches A and B showed similar crystallite sizes and lattice constants. The interesting part begins when looking at the lattice constants of the starting powder batches, the sintered PSN pellets and finally the annealed PSN samples. Between each step, the lattice constants consequently increased. Table 4.1.3 and Figure 4.1.22 shows a clear relationship between exposure to high temperature and lattice constant. Sample1, which was exposed to a high temperature for the longest time, also had the highest calculated lattice constant. While Sample2 and Sample3, annealed for 18 hours at 1100°C and 1150°C, showed the same trend with Sample3 having the largest lattice constant after annealing. After the sintering step, the samples also measured different lattice constants, although the lattice constant of the sintering powder was the same. Here, the fact that the pellets were placed on top of each other during sintering could have played an important role, in addition to the sample thicknesses. The pellets that were isolated on both sides should therefore have given the smallest lattice constant. In addition, the lower surface to volume ratio of Sample1 should be taken into account. Unfortunately, the position of the pellets were not noted for later use, but what we can indeed see from Table 4.1.3, is that two of the samples (Sample2 and Sample3) had quite lower density than the sintered Sample1. We may therefore assume that Sample2 and Sample3 were isolated the most, that is, they were on the bottom. Also, the thinnest of the samples during sintering would have larger surface to volume ratio, which then would naturally cause a higher vol% PbO to evaporate. Both these factors may have contributed to the different lattice constant after sintering. And this could then explain the reduced sintering (density decrease) of Sample1 during annealing, as it had already reached its "limit" with respect to PbO evaporation. The brighter areas close to the sides of Sample1

(see Figure 4.1.21) after annealing, may also be a sign of the lower density. In the same picture it can be seen that Sample3 has a more uniform color, in agreement with the higher density. An analogy to the above argumentation could be comparing the pellets to beef steaks, where Sample1 is the smallest one. Naturally, the smaller beef steak needs shorter time to be ready than two other larger steaks. Then when the two larger steaks are ready, it may be too late for the small one, as most of the water has evaporated and it has turned into a low density piece of coal. This is only a speculation but it may reflect some of the differences after sintering. The most important to take from the different lattice constants is that they all increase after heat exposure. PbO loss will therefore be considered the main contributor to the decreasing lattice constant. A theory will be presented to explain this, and also in the next section, how it may have affected the dielectric properties.

First we must become familiar with the crystal structures of ordered and disordered PSN crystal lattices. A disordered and ordered version of PSN are visualized in Figure 5.2.5 and 5.2.6. These are merely visualizations based on sizes of the cations. Bonding preferences are not included, but nevertheless, they may help explaining the coming hypothesis.

The figures illustrates how the thermodynamically favored distribution of Sc^{2+} and Nb^{5+} in ordered PSN may cause the structure to contract and therefore yield a smaller lattice constant as mentioned in the theory section. In a disordered PSN however, illustrated in Figure 5.2.5, we may visualize that the B' (grey) and B'' (green) octahedral sites are occupied by a random number of Sc^{2+} and Nb^{5+} ions, making the B' and B'' sites in a way equal. This may be thought of as the Sc^{2+} (white) and Nb^{5+} (black) ions occupying the B' and B'' sites equally (half black and half white). This illustration represents an "ideal" disordered situation only made to help explaining. But the consequence of the random B- cation distribution is the B'' octahedral sites being slightly too big for the Nb^{5+} ions. This is analogous to $PbTiO_3$ where the A- cation is large causing the TiO_6 octahedra to be slightly too big for the smaller Ti^{4+}. We can therefore imagine that this arrangement would lead to an unfavorable situation and a larger lattice constant. However, in an ordered PSN illustrated in Figure 5.2.6, the B' and B'' sites are occupied by different atoms, thus called B- site ordering. As we have learned they are occupied by Sc^{2+} and Nb^{5+} ions respectively in PSN. Because of the size and charge difference of the B- cations, the "pressure" from the larger Sc^{2+} ion can now be released by oxygen anions moving towards the Nb^{5+} cation. Although the distortion is exaggerated in Figure 5.2.6, it may help us understand why the ordered superstructure lattice constant is slightly smaller than that of disordered PSN.
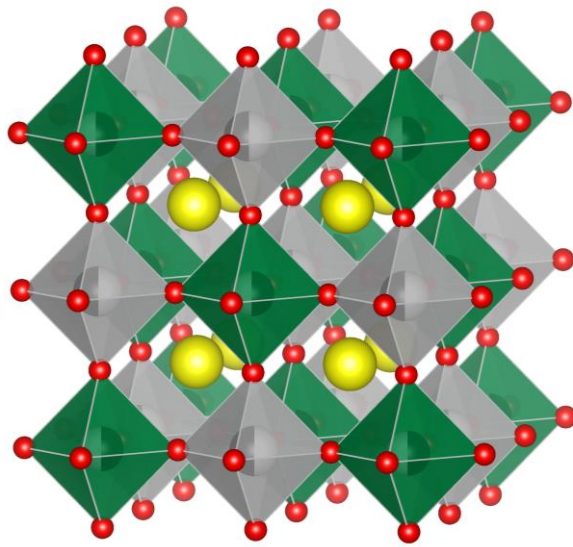
Figure 5.2.5 *Visualization of a disordered PSN (Pb(Sc$_{1/2}$Nb$_{1/2}$)O$_3$) perovskite. The B' and B'' octahedral sites are occupied equally by Sc^{2+} (white) and Nb^{5+} (black) atoms respectively. O^{2-} and Pb^{2+} are shown in red and yellow respectively. (Made with VESTA visualization software).*
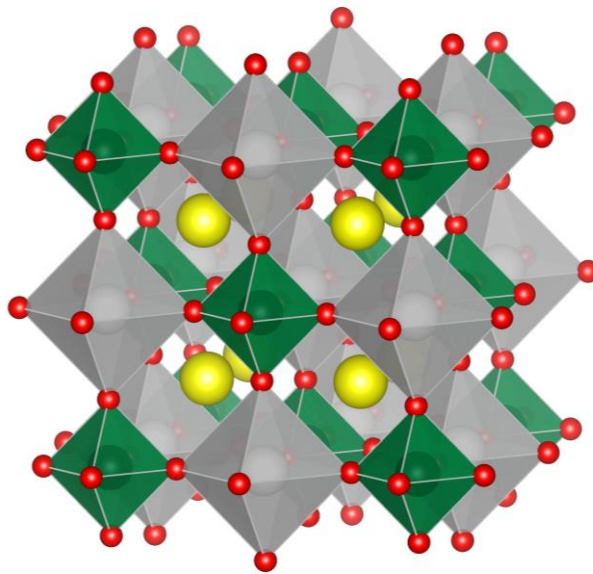
Figure 5.2.6 *Visualization of an ordered PSN (Pb(Sc$_{1/2}$Nb$_{1/2}$)O$_3$) perovskite. The B' and B'' octahedral sites are occupied solely by Sc^{2+} (white) and Nb^{5+} (black) atoms respectively creating an oxygen distortion towards the smaller Nb^{5+} ion. O^{2-} and Pb^{2+} are shown in red and yellow respectively. (Made with VESTA visualization software).*

And now to the hypothesis regarding the lattice constant increase in the experimental results. The proposed theory is that PbO evaporation introduces lead and oxygen vacancies (V_{Pb}'' and V_O^{**}), causing the crystal structure to expand slightly. To argument for this, we must first consider the effect of a vacancy. By removing a Pb^{2+} and O^{2-} we can imagine the vacancy sites becoming negative and positive for a Pb^{2+} and O^{2-} vacancy respectively, hence the writing V_{Pb}'' and V_O^{**}. As shown in Figure 5.2.5 and 5.2.6, the Pb^{2+} is surrounded by oxygen octahedra. Now if we were to remove a Pb^{2+} and leave a negative vacancy, this should according to electrostatics cause the vacancy to give a small push on the oxygen octahedra, separating them even more. Pb^{2+} can in that case be thought of as bond holding the oxygen octahedra together. But by removing this bond, and considering that the oxygen anions are negatively charged, we may expect that they also want to be farther apart. For this reason the lattice constant increase is believed to be caused by PbO evaporation. Other studies on PSN has also reported lower larger constants for vacancy containing or A- site substituted PSN, with vacancy PSN measuring a lattice constant of 4.082Å compared to 4.079Å [22].

The oxygen vacancy however, is believed to cause a displacement of the remaining oxygen anions to better screen the highly charged Nb^{5+} cation. This may be accomplished by the remaining anions moving closer to the Nb^{5+} cation. From this we see that we have two situations, with one expansion and one contraction. This argumentation is merely a hypothesis that may be used to explain both the increasing lattice constant and next, the dielectric properties. To support this theory, earlier study on $PbTiO_3$ also shows an increasing lattice constant as a function of PbO deficiency [53]. It should though be noted that the measured increase in lattice constant was smaller, and that it also seemed somewhat related to a contraction of the c- axis. The hypothesis of an induced screening of the Nb^{5+} cation is also supported by data on Nb^{5+} with coordination number (CN) 4 and 6, where a CN of 4 has the smallest ionic radius of 0.48Å compared 0.64Å [54].

Annealing effect on dielectric properties

For the best of the further discussion, the measured values of Sample1 only will be used and compared with respect to dielectric properties. The reason for this is the individual differences between the samples with respect to dimensions during measurements, density and position in the crucible during sintering. As we could see from Table 4.1.4, both Sample2 and Sample3 showed a reduction in T_m and an increasing frequency dependence. Sample2 followed the same trend as Sample1, while Sample3 showed a much larger dielectric maxima. A possible explanation to this would only be speculations and will therefore not be given.

Sample1 showed a reduction in T_m and ε'_m and an increasing frequency dependence upon annealing. The two effects mentioned first are seen for highly ordered PSN [29]. But, the fact that the frequency dependence ΔT_m was larger after annealing represents an increasing relaxor behavior, opposite to what was expected. However, earlier studies have also reported that lead evaporation may have the same effect on the dielectric properties as B- site

ordering [55]. Although we cannot confirm the hypothesis stated in the last section, we can indeed confirm that PbO evaporation is happening. The reduction in secondary phases after using a PbO excess are a good indication of lead evaporation, in addition to the swollen calcined PSN pellets. From these observations, we are in right to assume some degree of lead and oxygen vacancies.

From theory we know the effect of Pb^{2+} on raising T_C in $PbTiO_3$. It is therefore likely a similar stabilization mechanism also affects the behavior of PSN and this is also supported by literature on the topic [27]. Any other A- site cation or vacancy that replaces Pb^{2+} in $PbTiO_3$ is known to reduce the Curie temperature, and this is a well-known method in industry to obtain high dielectric constants at room temperature [1]. The experimental results in this study also showed an alteration of T_m, and from XRD data we could exclude cation ordering. Therefore, as earlier studies have confirmed it, and by the hypothesis of PbO causing an increasing lattice constant, PbO evaporation is the most probable cause. The interesting discussion begins now, in trying to explain the reason why.

Assuming that PbO evaporation left oxygen and lead vacancies, then this should also reduce the overall coupling between the Pb^{2+} and ferroelectric active Nb^{5+}, similar to a vacancy or A-site substitution in $PbTiO_3$. And in a similar way, the stabilization of the ferroelectric cation is removed and hence Nb^{5+} displacement should be easier affected by temperature, hence T_m is reduced. This temperature reduction may be viewed as a way to stabilize the cation in an off center position, and that the temperature decrease, increases the barrier height between those positions. A similar analogy was used by Chen *et al.* [27] where they concluded that losing this stabilization is responsible for T_m reducing upon ordering. In the same article, 1:1 ordering of Pb^{2+} was also considered an important part of the 1:1 ordering on the B- site. Therefore, by removing the A-site cation, should according to this also cause more disorder, and hence an increasing relaxor behavior. This way, the PbO evaporation explains the increasing relaxor behavior, as a Pb^{2+} vacancy would alter this 1:1 ordering. In addition it also explains the temperature reduction of the dielectric maxima as the stabilizing effect on Nb^{5+} off- centering is lost.

To explain the reduced dielectric maxima, a second hypothesis will be given. By using the illustrated PSN in Figure 5.2.5 and 5.2.6 and assuming PbO evaporation causes vacancies, a possible explanation may be visualized. We know for a fact that ordered PSN shows a lower dielectric maxima compared to disordered PSN [22]. Further on, the visualized ordered PSN shows a clear limited room for displacement compared to disordered PSN where the oxygen octahedral sites were slightly too large for the Nb^{5+} cation. With this in mind and by using the oxygen vacancy hypothesis stated above, an explanation may be in our hands. As stated, the oxygen vacancies causes a distortion of the remaining anions towards the Nb^{5+} to better screen the charge. By doing so, we may visualize that the Nb^{5+} cations now have less room for displacement like in an ordered PSN, and hence the polarization will be smaller upon an off- centering. Off-centering is here, the stabilized position of Nb^{5+} cation within the oxygen

"octahedra" (now consisting of only 7 anions). The dielectric constant, which is a measure on how much charge is moved, should therefore now be smaller.

6. Conclusion

Phase pure PSN can successfully be synthesized by the molten salt synthesis. Both the *Wolframite method* and the conventional mixed oxides method give a phase pure PSN. However, the *Wolframite method* proves more stable with respect to phase purity and is in that regard the most favored route. As for the B- site ordering, neither methods resulted in cation ordering although synthesis temperatures were kept well below the reported order-disorder temperature for PSN. The lack of ordering is thought to be related to the kinetics in the molten salt synthesis, and therefore a modified order- disorder temperature is believed to govern this system. For this reason, further experiments should include synthesis in molten salt solutions where cation mobility is lower. The different routes showed different reaction rates, most likely affected by the particle sizes of the precursor. The precursor is also believed to have increased the particle sizes of the resulting PSN particles due to the limited nucleation sites. The heating rates showed a similar effect on particle and crystallite sizes in both routes yielding smaller and bigger particle and crystallite sizes for fast and slow heating respectively. It was in addition found that small crystallite sizes resulted in smaller lattice constants, which can also be measured in ordered PSN. However, they were not as low as in ordered PSN and a significant correlation between crystallite size and lattice constant could not be found.

For the solid state synthesized PSN, the PbO excess revealed its importance from beginning to the end. Both the density and the purity of the PSN pellets were related to the excess PbO. Pyrochlore phases known to reduce the dielectric permittivity appeared when not using this sintering aid. Sintering aid, because it also increased the pellet density. Also, an interesting discovery in this study was the correlation between the increasing lattice constant and exposure to high temperatures. A possible explanation was given, and is thought to be related to PbO evaporation introducing vacancies causing electrostatic repulsion. The PbO evaporation, and lead and oxygen vacancies are also thought to have a great impact on the dielectric properties. As earlier studies have also confirmed, vacancies may reduce both the dielectric permittivity maxima and its temperature. The same tendency is observed for ordered PSN, but as no ordering could be observed from XRD data, the altering of the dielectric properties are believed to be caused by PbO evaporation. By combining both facts and earlier discoveries, and the use of visualized crystal structures, a possible explanation is proposed in the form of a hypothesis. It is believed that Pb^{2+} vacancies reduces the temperature of the dielectric maxima in a similar manner to the Curie temperature alteration in $PbTiO_3$. In addition, the oxygen vacancies are believed to reduce the room for displacement of the ferroelectric active Nb^{5+} due to the lowered coordination number.

Literature

1. West, A.R. and C. West, *Basic solid state chemistry*. Vol. 36. 1999: John Wiley & Sons Chichester.

2. King, G. and P.M. Woodward, *Cation ordering in perovskites.* J. Mater. Chem., 2010. **20**(28): p. 5785-5796.

3. Bokov, A. and Z.G. Ye, *Recent progress in relaxor ferroelectrics with perovskite structure.* Frontiers of Ferroelectricity, 2007: p. 31-52.

4. Setter, N. and L. Cross, *The contribution of structural disorder to diffuse phase transitions in ferroelectrics.* Journal of Materials Science, 1980. **15**(10): p. 2478-2482.

5. Davies, P. and M. Akbas, *Chemical order in PMN-related relaxors: structure, stability, modification, and impact on properties.* Journal of Physics and Chemistry of Solids, 2000. **61**(2): p. 159-166.

6. Polla, D.L. and L.F. Francis, *Processing and characterization of piezoelectric materials and integration into microelectromechanical systems.* Annual review of materials science, 1998. **28**(1): p. 563-597.

7. Baazi, J.S., *B- cation ordering in "relaxor" ferroelectric perovskites*, in *Department of Materials Science and Engineering*2012, Norwegian University of Science and Technology: Trondheim. p. 1-45.

8. Bokov, A.A. and Z.G. Ye, *Phenomenological description of dielectric permittivity peak in relaxor ferroelectrics.* Solid State Communications, 2000. **116**(2): p. 105-108.

9. Tilley, R.J.D., *Understanding solids: the science of materials*. 2004: Wiley.

10. Richerson, D., *Modern ceramic engineering: properties, processing, and use in design*. Vol. 29. 2005: CRC.

11. Cross, L.E., *Relaxor ferroelectrics.* Ferroelectrics, 1987. **76**(1): p. 241-267.

12. Haertling, G.H., *Ferroelectric ceramics: history and technology.* Journal of the American Ceramic Society, 1999. **82**(4): p. 797-818.

13. Kay, H., *Electrostriction.* Reports on Progress in Physics, 2002. **18**(1): p. 230.

14. Setter, N. and L. Cross, *The role of B-site cation disorder in diffuse phase transition behavior of perovskite ferroelectrics.* Journal of Applied Physics, 1980. **51**(8): p. 4356-4360.

15. Kong, L.B., T. Zhang, J. Ma, and F. Boey, *Progress in synthesis of ferroelectric ceramic materials via high-energy mechanochemical technique.* Progress in Materials Science, 2008. **53**(2): p. 207-322.

16. Akbas, M.A. and P.K. Davies, *Domain growth in Pb (Mg1/3Ta2/3) O3 perovskite relaxor ferroelectric oxides.* Journal of the American Ceramic Society, 1997. **80**(11): p. 2933-2936.

17. Montgomery, J.K., M.A. Akbas, and P.K. Davies, *1: 1 Ordered Domain Growth in Pb (Mg1/3Ta2/3) O3-La (Mg2/3Ta1/3) O3 Relaxor Ferroelectric Perovskites.* Journal of the American Ceramic Society, 1999. **82**(12): p. 3481-3484.

18. Farber, L., M. Valant, M.A. Akbas, and P.K. Davies, *Cation Ordering in Pb (Mg1/3Nb2/3) O3–Pb (Sc1/2Nb1/2) O3 (PMN–PSN) Solid Solutions.* Journal of the American Ceramic Society, 2002. **85**(9): p. 2319-2324.

19. Setter, N. and I. Laulicht, *The Observation of B-Site Ordering by Raman Scattering in A (B'B.* Applied spectroscopy, 1987. **41**(3): p. 526-528.

20. Swartz, S. and T.R. Shrout, *Fabrication of perovskite lead magnesium niobate.* Materials Research Bulletin, 1982. **17**(10): p. 1245-1250.

21. Bing, Y.-H. and Z.-G. Ye, *Synthesis and characterizations of the (1– x) Pb (Sc 1/2 Nb 1/2) O 3–xPbTiO 3 solid solution ceramics.* Journal of Electroceramics, 2008. **21**(1): p. 761-764.

22. Malibert, C., B. Dkhil, J. Kiat, D. Durand, J. Berar, and A. Spasojevic-de Bire, *Order and disorder in the relaxor ferroelectric perovskite (PSN): comparison with simple perovskites and.* Journal of Physics: Condensed Matter, 1999. **9**(35): p. 7485.

23. Perrin, C., N. Menguy, O. Bidault, C. Zahra, A. Zahra, C. Caranoni, B. Hilczer, and A. Stepanov, *Influence of B-site chemical ordering on the dielectric response of the Pb (Sc1/2Nb1/2) O3 relaxor.* Journal of Physics: Condensed Matter, 2001. **13**(45): p. 10231.

24. Kimura, T., *Molten Salt Synthesis of Ceramic Powders.* 2011.

25. Yoon, K.H., Y.S. Cho, and D.H. Kang, *Molten salt synthesis of lead-based relaxors.* Journal of materials science, 1998. **33**(12): p. 2977-2984.

26. Fuoco, L., D. Rodriguez, T. Peppel, and P.A. Maggard, *Molten-Salt-Mediated Syntheses of Sr2FeReO6, Ba2FeReO6, and Sr2CrReO6: Particle Sizes, B/B′ Site Disorder, and Magnetic Properties.* Chemistry of Materials, 2011. **23**(24): p. 5409-5414.

27. I-Wei, C., L. Ping, and W. Ying, *Structural origin of relaxor perovskites.* Journal of Physics and Chemistry of Solids, 1996. **57**(10): p. 1525-1536.

28. Poplavko, Y. *The nature of large dielectric constant of relaxors*. in *Applications of Ferroelectrics, 2004. ISAF-04. 2004 14th IEEE International Symposium on*. 2004. IEEE.

29. Zhu, M., C. Chen, J. Tang, Y. Hou, H. Wang, H. Yan, W. Zhang, J. Chen, and W. Zhang, *Effects of ordering degree on the dielectric and ferroelectric behaviors of relaxor ferroelectric Pb(Sc1/2Nb1/2)O3 ceramics.* Journal of Applied Physics, 2008. **103**(8): p. 084124-084124-6.

30. Davies, P., H. Wu, A. Borisevich, I. Molodetsky, and L. Farber, *Crystal chemistry of complex perovskites: New cation-ordered dielectric oxides.* Annu. Rev. Mater. Res., 2008. **38**: p. 369-401.

31. Lufaso, M.W. and P.M. Woodward, *Jahn-Teller distortions, cation ordering and octahedral tilting in perovskites.* Acta Crystallographica Section B: Structural Science, 2004. **60**(1): p. 10-20.

32. Anderson, M.T., K.B. Greenwood, G.A. Taylor, and K.R. Poeppelmeier, *B-cation arrangements in double perovskites.* Progress in solid state chemistry, 1993. **22**(3): p. 197-233.

33. Chen, J., H.M. Chan, and M.P. Harmer, *Ordering Structure and Dielectric Properties of Undoped and La/Na-Doped Pb (Mg1/3Nb2/3) O3.* Journal of the American Ceramic Society, 1989. **72**(4): p. 593-598.

34. De Mathan, N., E. Husson, P. Gaucher, and A. Morell, *Modification of the B-site order of PbMg13Nb23O3 ceramics by thermal annealing or by La-doping.* Materials research bulletin, 1990. **25**(4): p. 427-434.

35. Viehland, D. and J.F. Li, *Compositional instability and the resultant charge variations in mixed B-site cation relaxer ferroelectrics.* Journal of applied physics, 1993. **74**(6): p. 4121-4124.

36. Dmowski, W., M. Akbas, T. Egami, and P. Davies, *Structure refinement of large domain relaxors in the Pb(Mg1/3Ta2/3)O3–PbZrO3 system.* Journal of Physics and Chemistry of Solids, 2002. **63**(1): p. 15-22.

37. Yan, Y., S. Pennycook, Z. Xu, and D. Viehland, *Determination of the ordered structures of Pb3(MgNb)O9 and Ba3(MgNb)O9 by atomic-resolution Z-contrast imaging.* Applied physics letters, 1998. **72**: p. 3145.

38. Park, K., L. Salamanca-Riba, M. Wuttig, and D. Viehland, *Ordering in lead magnesium niobate solid solutions.* Journal of materials science, 1994. **29**(5): p. 1284-1289.

39. Caranoni, C., P. Lampin, I. Siny, J. Zheng, Q. Li, Z. Kang, and C. Boulesteix, *Cosmparative study of the ordering of B-S ite cations in Pb2ScTaO6 and Pb2ScNbO6 perovskites.* physica status solidi (a), 1992. **130**(1): p. 25-37.

40. Galasso, F. and W. Darby, *Preparation of single crystals of complex perovskite ferroelectric and semiconducting compounds.* Inorganic Chemistry, 1965. **4**(1): p. 71-73.

41. Ismailzade, I., *Results of a Preliminary X-Ray Examination of Samples of Pb(Nb1/2Sc1/2)O3 and Pb (Ta1/2Sc1/2)O3*, 1959, XristaZZografiya.

42. Stenger, C. and A. Burggraaf, *Order–disorder reactions in the ferroelectric perovskites Pb (Sc1/2Nb1/2) O3 and Pb (Sc1/2Ta1/2) O3. I. Kinetics of the ordering process.* physica status solidi (a), 1980. **61**(1): p. 275-285.

43. Glazounov, A. and A. Tagantsev, *A "breathing" model for the polarization response of relaxor ferroelectrics.* Ferroelectrics, 1999. **221**(1): p. 57-66.

44. Viehland, D., S. Jang, L.E. Cross, and M. Wuttig, *Deviation from Curie-Weiss behavior in relaxor ferroelectrics.* Physical Review B, 1992. **46**(13): p. 8003.

45. Cheng, Z.Y., R.S. Katiyar, X. Yao, and A.S. Bhalla, *Temperature dependence of the dielectric constant of relaxor ferroelectrics.* Physical Review B, 1998. **57**(14): p. 8166-8177.

46. Cheng, Z.Y., L.Y. Zhang, and X. Yao, *Investigation of glassy behavior of lead magnesium niobate relaxors.* Journal of applied physics, 1996. **79**(11): p. 8615-8619.

47. Grinberg, I. and A.M. Rappe, *Local structure and macroscopic properties in Pb(Mg1/3 Nb2/3)O3 - PbTiO3 and Pb(Zn1/3Nb2/3)O3 - PbTiO3 solid solutions.* Physical Review B, 2004. **70**(22): p. 220101.

48. Juhas, P., I. Grinberg, A.M. Rappe, W. Dmowski, T. Egami, and P.K. Davies, *Correlations between the structure and dielectric properties of Pb(Sc2/3 W1/3)O3 - Pb (Ti/Zr)O3 relaxors.* Physical Review B, 2004. **69**(21): p. 214101.

49. Scheel, H. and D. Elwell, *Stable growth rates and temperature programming in flux growth.* Journal of Crystal Growth, 1972. **12**(2): p. 153-161.

50. Davies, P., L. Farber, M. Valant, and M. Akbas. *Cation ordering and dielectric properties of PMN-PSN relaxors*. in *AIP Conference Proceedings*. 2000.

51. Costa, A., C. Galassi, G. Fabbri, E. Roncari, and C. Capiani, *Pyrochlore phase and microstructure development in lead magnesium niobate materials.* Journal of the European Ceramic Society, 2001. **21**(9): p. 1165-1170.

52. Perrin, C., N. Menguy, E. Suard, C. Muller, C. Caranoni, and A. Stepanov, *Neutron diffraction study of the relaxor-ferroelectric phase transition in disordered Pb (Sc1/2Nb1/2) O3.* Journal of Physics: Condensed Matter, 2000. **12**(33): p. 7523.

53. Selbach, S.M., T. Tybell, M.-A. Einarsrud, and T. Grande, *PbO-deficient PbTiO3: Mass transport, structural effects and possibility for intrinsic screening of the ferroelectric polarization.* Applied Physics Letters, 2011. **98**: p. 091912.

54. Shannon, R., *Revised effective ionic radii and systematic studies of interatomic distances in halides and chalcogenides.* Acta Crystallographica Section A: Crystal Physics, Diffraction, Theoretical and General Crystallography, 1976. **32**(5): p. 751-767.

55.   Chu, F., I. Reaney, and N. Setter, *Spontaneous (zero-field) relaxor–to–ferroelectric-phase transition in disordered Pb (Sc 1/2 Nb 1/2) O 3.* Journal of applied physics, 1995. **77**(4): p. 1671-1676.